Validation of an Augmented Parcel Approach for Hurricane Regional Loss Assessments

Tracy Kijewski-Correa[1], Barbaros Cetiner[2], Kuanshi Zhong[3], Chaofeng Wang[4], Adam Zsarnoczay[5], Yunhui Guo[6], Meredith Lochhead[7], Frank McKenna[8]

[1]Corresponding Author, Department of Civil & Environmental Engineering and Geological Sciences and Keough School of Global Affairs, University of Notre Dame, 236 Hesburgh Center for International Studies, Notre Dame, IN 46556, USA, tkijewsk@nd.edu

[2]Civil and Environmental Engineering, University of California, Los Angeles, 420 Westwood Plaza, 3771 Boelter Hall, Los Angeles, CA 90095, bacetiner@ucla.edu

[3]Department of Civil and Environmental Engineering, Stanford University, Panama Mall, Building 02-540, Stanford, CA 94305, kuanshi@stanford.edu

[4]M.E. Rinker, Sr. School of Construction Management, University of Florida, 573 Newell Dr., Gainesville, FL 32603, chaofeng.wang@ufl.edu

[5]Department of Civil and Environmental Engineering, Stanford University, 439 Panama Mall, Building 02-540, Stanford, CA 94305, adamzs@stanford.edu

[6]Electrical Engineering and Computer Sciences, University of California at Berkeley, 387 Soda Hall, Berkeley, CA 94720, yunhui@berkeley.edu

[7]Department of Civil & Environmental Engineering and Geological Sciences, University of Notre Dame, 156 Fitzpatrick Hall, Notre Dame, IN 46556, USA, mlochhea@nd.edu

[8]Department of Civil Engineering, University of California at Berkeley, Berkeley, CA 94720, fmckenna@berkeley.edu

Abstract

While simulation environments for the study of community resilience are rapidly advancing, they remain constrained by the completeness of inventory data. This paper presents an augmented-parcel approach leveraging various sources of open data, machine learning modules and time-evolving rulesets to support Hazus-compatible risk assessments on a wide class of buildings under hurricane wind and flood hazards. These techniques are implemented within the open-source regional hurricane loss assessment workflow of the NHERI SimCenter. Illustrative examples demonstrate building inventory generation in both data-rich and data-scarce

environments. The study's validations of computer vision-based modules underscore the importance of training on "in the wild" images labeled with explicit knowledge of the region and representative of architectural nuances such as carports. Validations further reveal the challenges of simplifying complex contemporary roof geometries to the simplified shapes adopted in Hazus and the criticality of accurate year built data, given the augmented parcel approach's reliance on time-evolving code-based rulesets. Published field observations collected in Lake Charles, LA following the landfall of Hurricane Laura demonstrate that the use of an augmented-parcel inventory within the SimCenter's workflow for Hazus-compatible loss assessments yields damage states consistent with ground-truth observations for minor to moderate damage states. Simulations of extreme damage states (characterized by fewer ground-truth observations) bias toward minor damage for undamaged structures and plateau at moderate damage even for severely damaged and collapsed buildings. This trend persists when considering uncertainty in hazard intensity, as well as the low rates of shutter compliance. Root causes of inconsistencies revealed in this validation exercise will require further processing of street-level panoramic images to generate more samples of severely damaged and collapsed buildings as well as post-2007 construction.

1.0 Introduction

Communities are routinely faced with the challenge of describing their inventories of buildings and other infrastructure assets. Ultimately the way in which inventories are described, and the fidelity and frequency with which those descriptions are updated, depends entirely on the end use of that data, creating challenges when that data is then leveraged for engineering analyses (Zsarnóczay et al. 2022). Some of the earliest forms of inventorying were driven by the need to assess value for the purposes of taxation, e.g., (Department of the Treasury 2018); it was only fitting that these same inventories were mobilized by the need to assess losses for the purposes of catastrophe. Soon the assessment of losses under different disaster scenarios, as either part of planning and preparedness or during response and recovery, e.g., (New Jersey Office of Emergency Management 2014), became a routine exercise in hazard-exposed communities, creating a new valuable end use for inventory data, e.g., (New Jersey Department of Environmental Protection 2019).

The generation of such inventories can be conceptualized as a classification exercise, where the degree of nuance required in the data model, and thus the number of fields, is dictated by the fidelity of the loss estimation approach adopted. While the Hazus general building stock has been engaged by scholars, practitioners and policymakers, it has inherent limitations with respect to the granularity and accuracy it affords (Shultz 2017). Developing a context-specific inventory capable of overcoming these limitations requires parsing data, often from a number of sources, to construct the inventory. Unfortunately, the completeness and reliability of the data exposed by local authorities varies widely, especially where governments have limited capacity to generate, maintain and expose even the most basic inventory data, challenging the notion of standardizing inventory generation using data sources that are relevant, consistent, and useful (Jaiswal and Wald 2008). Still, the efforts to create a global earthquake model have made important strides in cataloging the distribution of buildings in such environments based on material, lateral force resisting system, and occupancy type (Jaiswal et al. 2010), and the use of Bayesian updating based on open-source data has continued to evolve the capacity to classify occupancies (Stewart et al. 2016). For hurricanes, efforts like the Florida Public Loss Model have made important strides to both highlight the challenges of integrating diverse sources of data for catastrophe models and offer multi-faceted strategies to address the associated uncertainties (Pinelli et al. 2020). Other states like New Jersey have made similar strides in assembling critical data needed to assess risks due to hurricanes, with efforts centered on federating a large number of hazard and inventory data sources into singular geospatial environments (Kijewski-Correa et al. 2020). The Center for Risk-Based Community Resilience Planning has also worked on develop building inventories for testbeds exposed to different hazards, which include applications to tornadoes (Joplin, MO), hurricanes/coastal flooding (Lumberton, NC and Galveston, TX), and tsunamis (Seaside, OR), accessible through their IN-CORE platform (Center for Risk-Based Community Resilience Planning 2022), using a variety of methodologies developed by the Center (Rosenheim et al. 2021). Their efforts have highlighted the need for more precise building descriptions and potentially the purchase of inventories from third-party providers or the creation of inventories using tax appraiser data, which inevitably requires additional enrichment with structural data in order to be used for hazard risk assessment (Roohi et al. 2021). Tax appraiser data also inevitably has gaps in its reported fields, which may be addressed by manually interrogating Google Street View and satellite imagery or conducting a rapid visual screening in the field (Park et al. 2017), and further automated using deep learning approaches (Aravena Pelizari et al. 2021). Access to other data sources and models can further enrich the economic and demographic information associated with each parcel (Waddell 2002).

The issues surrounding the completeness and accuracy of available inventory data are only compounded by the fact that high-performance computing has now enabled the theoretical frontiers of loss estimation to move away from their origins as an aggregated measure of impacts to portfolios of buildings described by fragilities and toward the description of specific assets by physics-based models (Deierlein and Adam Zsarnóczay 2021). The exciting potential for increasing granularity and fidelity of loss estimation that can bring assessments down to the scale at which individual mitigation decisions are made will unfortunately outpace the existing inventory-generation mechanisms in municipalities, requiring new venues to characterize the growing list of required geometries, dimensions and components across thousands of buildings.

Fortunately, technological advancements are poised to address these challenges both by aiding municipalities in more efficiently generating and exposing valuable digital information and also maximizing the discovery potential from existing data sources. For example, fusions of blockchain technology (BCT) and building information modeling (BIM) are now streamlining post-disaster permitting (Nawari and Ravindran 2019) and thereby digitizing data critical to loss modeling. Meanwhile, innovations in computer vision and machine learning have helped to automate the digitization of inventories from aerial and surface imagery at various scales, from coarse spatial and fine temporal scales necessary to characterize the evolution of cities in data-scarce settings (Jaiswal et al. 2010) to finer spatial scales necessary to resolve features like soft-stories (Yu et al. 2019). As the lack of high-quality, parcel-level descriptions of building inventories could potentially stymie the rapid advances in computational simulation capabilities for high-fidelity loss assessment, continuing to advance the ability to automate the mining, enrichment and augmentation of existing data sources is vital to inventory development.

In response this paper offers the following contributions: (1) the introduction of an *augmented-parcel approach,* defined as a set of operations that enrich the information normally exposed for parcels within municipal databases. Augmented-parcel approach leverages existing open data, machine-enabled techniques, and heuristic rulesets grounded in local codes/standards and normative construction practices to automatically generate a suite of hazard and structural attributes necessary to conduct loss assessments and in a manner that is replicable and tractable over large-scale inventories. Illustrative examples in Atlantic County, NJ and Lake Charles, LA (2) demonstrate the real-world application of the augmented-parcel approach to generate large-scale inventories for Hazus-compatible loss assesssment, overcoming data deficits in settings with limited data availability. Finally, (3) validations throughout the paper demonstrate the performance of various parcel augmentation strategies using ground truth data and offer a validation of Hazus-compatible loss assessments using field observations gathered in Lake Charles, LA following Hurricane Laura. While the emphasis of this paper is regional hurricane loss estimation within a Hazus-compatible framework, given the opportunity to validate computer vision estimates of geometric features required for wind loss estimation, the methodologies and overall workflow are generalizable to other hazards and loss estimation approaches, as demonstrated by complementary efforts directed toward detecting features such as soft stories (Yu et al. 2020) and enabling component-based loss estimation in accordance with FEMA P-58 (Zsarnóczay and Deierlein 2020).

2.0 Overview of Augmented Parcel Approach

The transition from census-block-level loss projections to parcel-level projections of damage to individual buildings under hazard events demands a wider range of inventory data, though the specific building and hazard attributes required depend upon the hazards included in the analysis as well as the adopted loss modeling approach. The adoption of the Hazus loss modeling framework in this study demonstrates specifically how machine learning and computer vision techniques can be coupled with time-evolving heuristic rulesets grounded in local codes/standards and normative practice to generate the building information necessary to widen access to asset-level implementations of this de-facto loss modeling approach, regardless of a community's level of data readiness. Following the overall computational workflow in Wang et al. (2021a), this section describes the process of assigning attributes to a large-scale inventory of building footprints defined over a specific geographic region. The flow chart in Figure 1 illustrates the various phases of the augmented parcel approach described herein. Illustrative examples in the subsequent section will then introduce a pair of real-world inventories generated using this methodology.

2.1 Phase I: Attribute Definition

A generalized data model is first developed to organize the universe of attributes necessary to describe each of the building footprints. Attributes include all building, hazard and site features necessary to select the appropriate fragility curve in the Hazus wind and flood loss models, as well as any secondary variables that may be necessary to assign that attribute based on the data commonly reported in municipal building inventories used in tax assessment and permitting; these are organized under the building classes defined by Hazus. See the Supplemental Materials for a complete listing of the residential, commercial, industrial, agricultural, religious, government, education and essential facilities building classes defined for hurricane wind (Table A.1a), inundation (Table A.1b) and wave-induced (Table A.1c) hazards. The structural and hazard attributes required to assign fragility functions in Hazus wind and flood loss models for each supporting building class were subsequently inventoried and potential data sources and augmentation strategies were mapped to each attribute. While hazard attributes are often available from third party data (3PD), a review of inventories compiled in the data-rich NJcoast project (Kijewski-Correa et al. 2020) highlighted a number of structural attributes that were unlikely to be available in municipal data (MD); evaluation of data scarce communities in Louisiana suggested that even some basic property data may additionally need to be addressed through an augmentation strategy. Strategies to address these gaps were identified, including machine-enabled (ME) techniques and rule-defined (RD) assignments based on legacy building codes, local construction practices/norms, and human subjects data. By working backwards to map the finest level of data required to complete a Hazus loss assessment on a specific building footprint, secondary data required for rules-based assignments were also identified and included in a comprehensive data model. Supplemental Materials Table A.2 reports the resulting data model with fields grouped by category: *Building Information* for basic property data, *Construction Features* for largely geometric and dimensional data, *Hazard Attributes* for wind and flood-related hazard and site data, *Structural Attributes* for the data needed by Hazus wind and flood loss models (FEMA 2018a; b) to select appropriate fragility descriptions, and *Simulation Parameters* for regional simulation settings. The method(s) that can be used to populate each field are also mapped in Table A.2 and detailed in the following subsections, in some cases providing multiple potential approaches, with some values either default assigned (A) or derived (D) from other fields.

2.2 Phase II: Initial Population

The data model developed in Phase I is then initially populated by web scraping available open-data sources to populate as many fields as possible (refer back to Table A.2 for list of fields associated with MD and/or 3PD designations). Available municipal data such as tax appraiser and permit databases may contain most Building Information data fields, as well as some Construction Features, however, there are considerable challenges in accessing the data required for loss estimation (Zsarnóczay et al. 2022). As the data are generated and maintained in a fragmented manner, possibly without the enforcement of county/parish or statewide data standards, there is wide variation in the fields reported, their completeness, and accuracy. As the case studies later in this paper demonstrate, some states have invested in expanding the data reported for the purposes of hurricane loss estimation and floodplain management (what we term *data rich* environs), whereas other states may be in their infancy in exposing even the most basic building information (what we term *data scarce* environs). More standardized data is available nationwide to support hazard/exposure descriptions, e.g., FEMA Flood Insurance Rate Maps (FIRMs), Land Use Land Cover (LULC) databases, and the Applied Technology Council (ATC)'s Hazards by Location Application Programming Interface (API) (Applied Technology Council n.d.), which can be used to populate many Hazard Attributes.

2.3 Phase III: Machine-Enabled Attribute Assignment

A range of machine-enabled techniques were then developed to populate missing Building Information and Construction Features. These modules are available through the NHERI SimCenter as part of CityBuilder, a python application that incorporates different artificial intelligence (AI)/machine learning (ML) modules from the center's backend tool BRAILS (Wang et al. 2021b). Each module's subsequent presentation includes a description of the methodology and associated validation process.

2.3.1 Roof Shape

The roof shape (Attribute: *RoofShape*) is considered a high-priority attribute both for importance in assessing wind vulnerability but also its limited reporting in standard open municipal data. Thus an image classifier operating on available satellite imagery (e.g., Google Maps) was developed using the convolutional neural network (CNN) ResNet50 (He et al. 2016). The classifier was trained to assign roof images for each building footprint to one of three categories used in Hazus: gable, hip, or flat. The original training of the AI model utilized 6,000 images obtained from Google satellite imagery in conjunction with roof labels obtained from OpenStreetMap (OSM). The training set was distributed equally across the three roof types, i.e., 2,000 images labeled as 'flat', 'gabled', and 'hipped', respectively. During the development of the model, 80% data was used for training and 20% was used for testing. As many roofs have more complex shapes, a similitude measure is used to determine which of these roof geometries is the best match to a given roof, with full details and the trained model released as part of the BRAILS backend component (SimCenter 2022). The classifier was then validated using a cleaned dataset of 125 unobstructed satellite images sampled nationwide from OpenStreet Maps. The selected roof images were screened to match the idealized gable, hip and flat geometries adopted by Hazus in order to establish the efficacy with which these three fundamental roof shapes could be identified from publicly available satellite imagery, achieving a detection rate of 93.15% across all three roof classes Wang (2021a). However, it is important to note that over time, roof geometries have become increasingly more complex, blending traditional hip and gable forms that deviate significantly from the idealized shapes adopted by Hazus. While the classifier's similitude measure negotiates this reality by forcing these complex roofs into one of these simple geometries, performance of a Hazus-consistent roof classifier will inevitably see a degradation in performance when applied to inventories with more complex roof geometry, as discussed further in *StEER Validation Exercise* for Lake Charles, LA following Hurricane Laura.

2.3.2 Building Dimensional Data

The roof dimensions (Attributes: *MeanRoofHt, RoofSlope*) and other building elevation data (Attributes: *ElevationR0, ElevationR1, FirstFloorHt, FirstFloorHt1, NumberOfStories*) are also considered high-priority attributes not reported by most open municipal data but critical to classifying hurricane-vulnerable buildings. Generating such critical dimensional data requires identification of the building stories and their relative elevations.

A detection model that can automatically detect rows of building windows was established to generate the image-based detections of visible floor locations from street-level images. The model was trained on the EfficientDet-D7 architecture (Tan et al. 2020) with a dataset of 60,000 images, using 80% for training, 15% for validation, and 5% testing of the model. In order to ensure faster model convergence, initial weights of the model were set to model weights of the (pretrained) object detection model that, at the time, achieved state-of-the-art performance on the 2017 COCO Detection set (Lin et al. 2014). For this specific implementation, the peak model performance was achieved using the Adam optimizer (Kingma and Lei Ba 2014) at a learning rate of 0.0001 (batch size: 2), after 50 epochs.

For a given Google Street View image of a building in the inventory, the floor detection model generates a bounding box output for its detections and calculates the confidence level associated with each detection (see Fig. 2). A post-processor that converts stacks of neighboring bounding boxes into floor counts was developed to convert this output into an estimate of the number of stories. An image may contain multiple buildings; therefore, this post-processor was designed to perform counts for each building in an image by clustering the bounding box detections for every building. When multiple buildings are encountered in an image, the post-processor yields multiple floor counts in the order the buildings are detected from left-to-right.

To validate performance, a test set was established by randomly selecting 3,000 parcels for which the number of floors was reported from the New Jersey Property Tax System Database (Department of Treasury 2018), called MODIV. These samples were drawn randomly from all counties of New Jersey, except Atlantic County, as this county is the site of one of the illustrative examples discussed later in this paper. Figure 3 provides the confusion matrix of model classifications, where a diagonal value of 1.0 indicates perfect classification. Validation against images with arbitrary camera orientations (termed “in the wild” images) results in 86% accuracy in classifying the number of stories (Fig. 3a). Validation using only “cleaned” images, where the building of interest is captured with minimal obstructions from trees or cars, is at the center of the image, and perspective distortions are limited, results in a detection accuracy of 94.7% (Fig. 3b).

Once the floors of a building are detected, the elevation of the bottom plane of the roof (lowest edge of roof line) and elevation of the roof (peak of gable or apex of hip) must be estimated with respect to grade (in feet) from street-level imagery (e.g., Google Street View), in order to estimate the roof height and mean roof height by respectively taking the difference or average of these elevations.

As in any single-image metrology application, extracting the building elevations from imagery requires: (1) rectifying image perspective distortions, typically introduced during image capture; (2) determining the pixel counts representing the distances between ends of the objects or surfaces of interest (e.g., for first floor height, the orthogonal distance between the ground and first-floor levels); (3) converting these pixel counts to real-world dimensions by matching a reference measurement with the corresponding pixel count.

Given that the number of street-level images available for a building can be limited and sparsely spaced, a single image rectification approach was deemed most applicable for regional-scale inventory development. The first step in image rectification requires detecting line segments on the front face of the building. This is performed by using the L-CNN end-to-end wireframe parsing method (Zhou et al. 2019). Once the segments are detected, vertical and horizontal lines on the front face of the building are automatically detected using RANSAC line fitting (Fischler and Bolles 1981), based on the assumptions that line segments on this face are the predominant source of line segments in the image and the orientation of these line segments change linearly with their horizontal or vertical position depending on their predominant orientation. The other support vector model implemented for image rectification focuses on the street-facing plane of the building in an image, and, based on the Manhattan World assumption (i.e., all surfaces in the world are aligned with two horizontal and one vertical dominant directions), iteratively transforms the image such that horizontal edges on the facade plain lie parallel to each other, and its vertical edges are orthogonal to the horizontal edges.

In order to automate the process of obtaining the pixel counts to then determine the elevation of identified stores, a facade segmentation model was trained to automatically label ground, facade, door, window, and roof pixels in an image. The segmentation model was trained using DeepLabV3 architecture on a ResNet-101 backbone (Chen et al. 2017), pretrained on PASCAL VOC 2012 segmentation dataset (Everingham et al. 2012), using a facade segmentation dataset of 30,000 images supplemented with relevant portions of ADE20K segmentation dataset. The peak model performance was attained using the Adam optimizer (Kingma and Lei Ba 2014) at a learning rate of 0.001 (batch size: 4), after 40 epochs. The conversion between pixel dimensions and real-world dimensions were attained by use of field of view and camera distance information collected for each street-level imagery. The identification of these elevations then enables the derivation of other attributes such as the *RoofSlope*, calculated as the ratio between the roof height and the roof run (defined as half of the smallest plan dimension of the building footprint).

2.3.3 Occupancy Class

In some data-scarce environments, occupancy data (Attribute: OccupancyClass) essential to assigning standard Hazus Building Classes may be unavailable or missing for a number of parcels in tax assessor data, prompting the development of an occupancy classifier. While the classifier can be expanded to encompass the full suite of Hazus Building Classes, it was initially developed to separate residential buildings: RES1 (single-family residence) and RES3 (multi-family residence), and general COM (commercial) buildings that encompass all defined commercial classes in Hazus (COM1-COM10). The occupancy classifier employs a convolutional neural network, trained using 15,743 Google Street View images with labels derived from OpenStreetMaps and an enriched inventory created by the New Jersey Department of Environmental Protection (NJDEP), discussed later as one of the paper's illustrative examples. The distribution of occupancies and sources of labels are summarized in Table 1.

The performance of the classifier was first validated against a ground truth dataset that contains 293 Google Street View images from the United States with labels from OpenStreetMap (98 RES1, 97 RES3 and 98 COM1 buildings) with unobstructed views of the buildings (cleaned data), which one can consider as examples of these occupancy classes that are easily identifiable by non-expert human agents. The confusion matrix, which presents visually the predictions versus actual data with ideal classification as 1.0 on the diagonal, is as shown in Figure 4a. A second validation is conducted using 3000 randomly sampled RES1, RES3 and COM buildings in the NJDEP dataset (1000 for each class). Google Street View images are downloaded for each sampled building. While classifying with accuracies as high as 99% for the OpenStreetMap testing dataset, classification accuracy diminishes for the NJDEP validation (Fig. 4b) due to two likely causes. First OSM validation data is cleaned whereas NJDEP is validating against a more realistic condition of "in the wild" images permitting obstructions, which will understandably reduce classification accuracy across all occupancies. Second, OSM labels were assigned semantically, without direct knowledge of the building, and thus the model is trained on commercial construction that was easy to visually identify by human agents. NJDEP data is locally-generated by officials whose classifications include non-semantic knowledge, based not upon appearance, but zoning, tax and other property information. This underscores the value of having access to reliable regional data labeled with direct knowledge of building function/occupancy when training image classifiers for this task. Further, the classifier was trained on images of common commercial buildings, and similar to the roof classifier, would necessarily assign each one of three classes (RES1, RES3, or generic COM) to every building it encounters. The generalization of occupancy to three classes in order to separate residential from non-residential construction should expect to see degraded performance when encountering buildings outside of traditional commercial construction. Though not explored herein, in municipalities where at least some building attributes are reported, multi-modal learning approaches fusing computer-vision and available building attributes may prove fruitful in classifying occupancy as well as assigning other missing attributes. Further, training a model to classify non-residential occupancy with greater nuance based on imagery alone presents practical challenges considering the diverse non-residential occupancies formalized in Hazus (see Supplemental Materials Table A.1a). Since these diverse classes of non-residential construction make up a small fraction of building inventories, there are inevitable limits on the amount of reliable training data available.

2.3.4 Year Built

One of the most critical features for the augmented parcel approach is the year built (Attribute: *YearBuilt*), given its essential role in the heuristic rulesets that assign many construction details necessary for loss estimation. Unfortunately, this attribute is not always reported in data-scarce communities. In such situations, third-party data sources like the National Structure Inventory (NSI) can be mined to extract this field for geocoded addresses across the United States. However, it should be noted that not all buildings are included in the NSI dataset, and the geocodes of the addresses may not align with building locations defined by available footprint data. As theorized in Wang et al. (2021a), a neural network can be used to predict the year built information for each building based on the spatial patterns learned from the NSI dataset. The

SimCenter's SURF application (Wang, 2019) is therefore employed to construct and train a neural network on the available NSI year built information within the inventory's geographic boundaries, allowing a *YearBuilt* assignment to be made at each footprint within that domain. In an effort to validate this approach, the authors used real estate websites (Zillow) to identify YearBuilt information for buildings listed on the market within the inventory domain. It is assumed that real estate listings, which require legally binding disclosures of building information, can be treated as "ground truth" in instances where tax assessor data is not available. This validation exercise was conducted in Lake Charles, LA, resulting in 1182 listings that were then used to train a neural network to generate YearBuilt values at all footprints for which a companion NSI-trained model had already predicted values. Figure 5a shows a scatter plot of the NSI-predicted year built against the Zillow-scraped results; while perfect agreement would cluster along the solid diagonal, the predicted year built data have a R2 value of 0.60 with respect to the Zillow data. The dashed lines in the figure define the 10-year boundaries about the perfect agreement line. As Phase IV will use time-evolving rulesets largely driven by code eras, YearBuilt must be estimated more accurately in the modern code era, which is post-2006 in Louisiana, and with a precision less than 10 years (depending on the frequency of code adoption/amendment cycles in a state/municipality and how much structural requirements change in each cycle). Note that the SURF-predictions trained on NSI data bias toward newer YearBuilt, which may result in predictions of less vulnerability using rulesets grounded in model building codes. These implications will be discussed further in *Hurricane Laura Verification & Validation Exercise.*

2.3.5 Attached Garage

As failures of attached garages can propagate damage into the primary structure, the presence of garages (Attribute: *Garage*) is critical to accurate loss assessments in residential construction, though not commonly reported in open-city data. A garage detector was trained to conduct a binary classification based on the presence of an attached garage in Google Street View imagery (which includes both detached garages and homes with no garage). The model was trained on the EfficientDet-D4 object detection architecture (Tan et al. 2020) using a subset of the SimCenter Labeled Building Facades dataset (Wang et al. 2021a). This subset comprises 1,887 Google Street View images from California, New Jersey, and Louisiana, sites of the SimCenter's regional simulation testbeds, and was utilized such that 80% of the images were marked for training, 10% for validation, and 10% for testing of the model. All of these images were pre-screened before model training to ensure that the buildings in the images are minimally occluded and are not heavily distorted. Similar to the number of stories detector, initial weights were set to model weights of the (pretrained) object detection model that, at the time, achieved state-of-the-art performance on the 2017 COCO Detection set (Lin et al. 2014). For this task, the peak detector performance was attained using the Adam optimizer (Kingma and Lei Ba 2014) at a learning rate of 0.0001 (batch size: 2) after 25 epochs. The classification includes a bounding box that expresses the confidence associated with the detection. A post-processor converts bounding box detections into garage existence information, with the ability to parse garages for multiple building instances in a single input image, as demonstrated by Figure 6, which also highlights the variation in confidence resulting from the presence of obstructions like vehicles and garbage cans. The model was validated on two datasets. The first used the validation subset reserved during initial training (N=189), which yielded the confusion matrix in Figure 7a showing 92% accuracy in detecting attached garages. A second validation was conducted using 300 randomly selected and manually labeled Google Street View images from Lake Charles, LA (Fig. 7b), the site of one of the illustrative examples later in this paper. In this region, attached garage detection drops to 82%, with "no garage" scenarios detected with 62% accuracy.

A deeper look at the differences between the training data used to generate the garage detection model and Lake Charles building inventory provides explanations for the discrepancy between the accuracies observed for the two validations. First, compared to denser urban environments, Lake Charles has a higher density of carports that may share the home's primary roof line, but are not fully enclosed with a door. The lower garage detection rates are likely due to the fact that this regional garage type was underrepresented in the training dataset. Moreover, most suburban homes in Lake Charles are architecturally unique in comparison to those in the initial training data, which may have affected "no garage" detection accuracy. Although a detection model can typically compensate for such differences, since the training data was drawn from three different states, the model understandably was unable to extrapolate well to the different building appearances in the Lake Charles building stock. It is important to note that none of the issues discussed above point to deficiencies in deep learning models but rather the need for representative training data in each region to recalibrate models to the architectural nuances in a given community.

2.4 Phase IV: Augmentation by Heuristic Rulesets

Basic building information scraped from municipal inventories in Phase II or mined from imagery in Phase III offer basic descriptions of a building and even geometric/dimensional data, e.g., single family home, made of wood, 1-story, but these are not the attributes the adopted loss model (Hazus) ultimately requires to determine damage and loss, e.g., secondary water resistance or roof-deck attachment. Thus the challenge lies in inferring these more granular attributes associated with the primary load path or water-resistant envelope from the data available in Phases II and III. The specific attributes required by Hazus also vary based on the building class, e.g., a wood single family home is described by five such attributes while a masonry version of the same home requires the assignment of up to three additional attributes. This thus requires a first step of assigning each footprint to a relevant Hazus building class based on the data generated in Phases II and III, followed by the assignment of required attributes for that footprint based on its building class. Thus three families of rulesets were developed to infer the Hazus building class and class-specific attributes for Hazus wind and flood loss models from data generated in Phases II and III. Rulesets include two aspects: the formal logic that evaluates various combinations of data from Phase II and III to determine the appropriate attribute assignment (including provenance metadata for any references used to justify the assignment), and then its implementation in Python for execution in the loss estimation workflow. The former is published on DesignSafe (Kijewski-Correa et al. 2022) and the latter in GitHub (Angeles et al. 2021).

The first family of rulesets is used to assign each footprint to a corresponding Hazus building class. For wind losses, buildings are grouped by primary building material (wood, masonry, concrete, steel, manufactured home) and then subclassified into one of fifty-five corresponding Hazus building classes (Table A.1a) and rulesets make this determination based on the occupancy, number of stories and plan area. For flood losses, rulesets assign one of thirtytwo building classes based on the occupancy, number of stories and foundation type (Table A.1b). For wave-induced losses, footprints are assigned to one of ten classifications by rulesets that consider building use, construction material and number of stories (Table A.1c). The rulesets include a default building class for each hazard if footprints are lacking one or more fields required to make the assignment. The defaults and formal logic are published for the 97 Hazus building classes on DesignSafe (Kijewski-Correa et al. 2022); the Supplemental Material Tables A.1a-c include an example of these rules to illustrate the process.

Next, rulesets were developed for each building class in the Hazus wind, flood and wave loss model to infer the required features, like roof to wall connection, from building and site information generated in Phase II and III. Whenever possible, the formal logic for these assignments derived from a review of the legacy building codes/standards (CS), creating rules that were time varying based on the requirements of different code eras in that regions. For attributes not specified by code, online research was conducted to determine likely construction practices/norms (PN) used in these code eras. As some attributes like use of window shutters requires agency on the part of homeowners, rates of compliance in existing human-subjects surveys (HS) where used to assign these attributes (Javeline and Kijewski-Correa 2019). When the attribute was expected to change over time, either based on changes in codes/standards for industry practices/norms, the rules are written as a function of YearBuilt, assigning attributes based on the governing code edition or availability of specific mitigation measures in the market at the time of construction. In cases where engineering judgment was required, rules were assigned based on the authors' understanding of the most common construction practices in a given region or conservative adoption of the most vulnerable configuration. In cases where variability is expected, attributes may be assigned as random variables (RV). Table 2 lists the methodological basis for the attributes used in Hazus wind and flood loss assessments, with some Direct Assignment (DA) of attributes based on attributes determined in Phases II and III. Note that some attributes may be assigned by multiple techniques based on the Year Built and eras when norms shifted or code requirements took effect, e.g., CS methods may apply in the modern code era, whereas PN or HS methods may govern in the era predating modern codes. Rulesets for each of the attributes in Table 2 again include default assignments in instances where one or more fields required by the ruleset are missing for that footprint, in which case attributes associated with an archetype building for that building class are assigned. The defaults and formal logic are published for the Hazus building classes on DesignSafe (Kijewski-Correa et al. 2022); the Supplemental Material Table A.2 includes an example of these rules to illustrate the process.

3.0 Illustrative Examples

Two illustrative examples are now presented to demonstrate the application of the above inventory generation processes at the municipal- and county-level. In either case, the process initiates with identification of building footprints, which should be preferably sourced from open governmental data generated with human oversight. Third-party footprint data may be necessary (Microsoft 2021), though hand-digitized footprints, e.g., 2017 Microsoft footprints, are preferable over computer-generated footprints, e.g., 2018 Microsoft footprints, that may fail to discern individual buildings in multi-building complexes/parcels. All data is ultimately georeferenced to the coordinates at the centroid of these footprints. BRAILS CityBuider application was used to develop the building inventories and assemble accompanying satellite and Street View imagery associated with each footprint for use in subsequent computer vision tasks (Wang et al. 2021b). Note that tax assessor data, one of the most valuable municipal data sources used in Phase II of inventory generation, is specified at the parcel level; parcels may contain multiple footprints and/or a footprint may cross multiple parcels, in which case rules used by the NJDEP were used to assign parcel attributes to those footprints (New Jersey Department of Environmental Protection 2019).

3.1 Scenario 1: Data Rich Environments

Many coastal communities have made substantive investments in open data that benefit a number of planning, emergency response and service delivery functions at the state and local level; among these is the State of New Jersey. Notably the New Jersey Geographic Information Network (NJGIN) has open access to federated data from different state agencies and counties to centralize base/hazard maps and datasets supporting emergency response, transportation, hazard assessments, and public works (Kijewski-Correa et al. 2020). Grant programs following Superstorm Sandy have helped many municipalities contract local firms to create GIS endpoints with local versions of these and other datasets describing their properties/parcels, infrastructure assets, planning/zoning polygons, and flood-vulnerability, e.g., repetitive loss structures and elevation certificates. The substantive investment in open data following a major damaging storm made this an ideal data-rich scenario for inventory development. Ultimately, Atlantic County, NJ and specifically Atlantic City and its surrounding municipalities were adopted as a case study, noting that this region is under active redevelopment with questions of resilience to climate-driven hazards of particular concern. The built environment in this region is quite diverse with a blend of low-rise commercial (1-3 stories), industrial, high-rise hotels/casinos (over 20 stories), and single/multi-family residences in a fairly compact geography. Thus this inventory can encompass both extremes in building typologies vulnerable to wind: wood frame single-family homes and tall flexible structures. From the perspective of hazard exposure, this region is also characterized by beachfront communities exposed to storm surge and breaking waves on the ocean-facing coastline coupled with back bay and riverine flooding.

A pair of inventories was developed in this region to allow the targeted investigation of flood-exposed properties as well as a wider study inclusive of properties outside the floodplain. Inventory development initiated with NJDEP Footprint Data, which includes flood-exposed properties cataloged in two geodatabases encompassing approximately 453,000 footprints across the entire state inclusive of all building footprints within the 1% annual chance (AC) floodplain, as defined by FEMA FIRMs as well as footprints that fall within a 200-ft buffer of the 1% AC floodplain boundary. These databases were combined and then clipped to retain only those within the limits of Atlantic County to form the *Flood-Exposed Inventory*. Half of this inventory's 32,828 buildings is derived from the three most populated municipalities in Atlantic County: Atlantic City, Margate City, and Ventor City, with 30,827 residential buildings and the remainder dominated by other occupancies such as commercial (N=1496) and governmental (N=7338) buildings. The majority are two-story (60%) or single-story (25%) construction, with wood as the dominant construction material (94%), with some masonry (3%) and concrete (3%) typologies. This inventory was then extended to include the remaining footprints within Atlantic County, with the Microsoft Footprint Database (Microsoft 2021) as the primary source of non-NJDEP footprint polygons. A separate roof segmentation algorithm (Durnov 2020) was applied to Google satellite images to parse multiple footprints out of errant singular footprints for multi-building parcels. This resulted in the full *Atlantic County Inventory.* This larger inventory is comprised of 100,721 buildings across the 23 municipalities of Atlantic County, with 90,017 residential buildings and the remainder dominated by other occupancies such as governmental (N=7338) and commercial (N=2366) buildings. With some tall buildings in Atlantic City, the vast majority are single story (91%) or two-story (6%) construction, with wood as the primary construction material (88%), followed by concrete (11%). This inventory pair is shown in Figure 8.

NJDEP also enriched its floodplain footprints with various attributes necessary to conduct standard FEMA risk assessments. All footprints included a set of Basic Attributes inclusive of parcel and site data and then Advanced Attributes required by Hazus User Defined Facilities (UDF) Module, which includes material, occupancy, replacement value, year built, area, number of stories, first floor height, and foundation type (New Jersey Department of Environmental Protection 2019). The augmentation also included data required by the FEMA Substantial Damage Estimator (SDE) Tool classifying residential superstructure, foundation, roof cover and exterior finishes. Thus the initial population of the data model for these two inventories exploited this augmented data to assign relevant fields to all properties in the floodplain (100% of buildings in the Flood-Exposed Inventory and that same subset within the Atlantic County Inventory, which was approximately one third of that larger inventory). For footprints not included in the NJDEP augmented datasets, these fields were assigned by parsing MODIV data, which is the New Jersey Tax Assessor Data (New Jersey Geographic Information Network 2021) with reference to the MODIV User Manual (Department of the Treasury 2018). Specifically, *OccupancyClass, BuildingType* (construction material) and *FoundationType* were parsed from MODIV data using the aforementioned heuristic rulesets (Angeles et al. 2021), with default values for any footprints where the required MODIV fields were lacking. Inclusion of a wide range of occupancies (see Supplemental Materials Table A.1a-c) required additional third party data from NJGIN Open Data portal to establish locations of essential facilities (using critical facilities layers) and define terrain characteristics using basic transformations of Land Use Land Cover data. Machine-enabled techniques introduced in Section 2.3.2 were then leveraged to estimate *NumberofStories* for all Atlantic County Inventory footprints not previously augmented by NJDEP, noting that this attribute tends to be under-reported in the MODIV database. Meanwhile *RoofShape*, assorted building elevation fields (as well as all derived roof dimensions), and *WindowArea* (assuming the proportion of windows on the front face is representative of the proportion on all faces) were respectively augmented by the machine-enabled techniques in Sections 2.3.1 and Section 2.3.2 for both the Flood-Exposed Inventory and the Atlantic County Inventory. Full details of the resulting data model and rulesets, with full provenance information, have been released on DesignSafe (Kijewski-Correa et al. 2022). The diversity of occupancy, number of stories and year of construction encompassed by this pair of inventories is affirmed by the statistical summaries in Figure 8.

3.2 Scenario 2: Data Scarce Environments

The process used in New Jersey was repeated in Lake Charles, LA to demonstrate how to efficiently generate inventories for the study of impacts and recovery following Hurricane Laura. Emphasis was placed on wind damage to residential construction, given the potential for validation exercises discussed in the next section. The attributes required for this class of construction were downsampled from the full data model presented previously in Supplemental

Materials A.2a and source data was identified. Unfortunately, there was a scarcity of open data in Lake Charles and Calcasieu Parish, requiring the use of machine-enabled approaches to assign the *YearBuilt* and *OccupancyClass*. While Louisiana has different code eras and code amendments that would require adaptation of the initial rulesets developed for Scenario 1, the rulesets from New Jersey were directly applied since both states employ IBC for contemporary construction. Beyond differences in the effective dates for specific years when code revisions became effective, Louisiana had no statewide code prior to 2006 and currently enforces 2015 IBC, with critical amendments related to wind speed caps in 2014, 2015, and 2017, and a freeboard cap in 2018, based upon the state's numerous hurricane recovery experiences; whereas New Jersey adopted statewide codes much earlier (1975), including IBC since 2003 and currently enforces 2018 IBC. With losses from Superstorm Sandy dominated by storm surge, New Jersey did not have the same intense periods of amendments to design wind speeds, making it well-suited to serve as the model for ruleset development with codes following the typical 3-year adoption cycle. While direct translation of the New Jersey rulesets without modification may result in predictions of better performance in Louisiana buildings constructed before 2006, extending effort to revise the New Jersey rulesets for this example was not warranted given the lack of reliable data on *YearBuilt* and *OccupancyClass* required for ruleset execution. The inventory and associated rulesets were further constrained to wood residential properties within the city limits of Lake Charles, LA (keeping 26,516 of the total 30,072 properties) and supporting only Hazus Building Classes WSF1-2 and WMUH 1-3 (see asterisks in Table A.1a indicating the retained classes). Figure 9 visualizes the geospatial distribution of *YearBuilt* in the resulting residential inventory with inset statistical distributions of key attributes. An additional cluster of homes south of Lake Charles was also included in the inventory to support subsequent validation exercises (this cluster and another within the city limits are shown in the inset in Fig. 9). Notably, this residential inventory is typified by older vintages of construction (pre-1980) (85%), with a dominance (98%) of low-rise (1-2 story) buildings and single-family (81%) residences. See asterisks in Table A.2 for fields retained in the downsized data model; details of the resulting data model and rulesets, with full provenance information, have been released on DesignSafe (Wang et al. 2021c).

4.0 Hurricane Laura Verification & Validation Exercise

Validation of the augmented parcel approach to generate inventories in support of hurricane loss assessment leverages the Lake Charles, LA inventory introduced under Scenario 2 to study the impacts of Hurricane Laura. As detailed in Roueche et al. (Roueche et al. 2020), the storm made landfall as a strong Category 4 hurricane near Cameron, LA in the early hours of 27 August 2020, tying the Last Island Hurricane of 1856 as the strongest landfalling hurricane in Louisiana history. Wind speeds are estimated to have reached or exceeded the design wind speed for Risk Category II buildings and other structures, as defined in ASCE 7-16 (American Society of Civil Engineers 2017) and the 2018 International Building Code (MRI = 700 years) (International Building Code 2018), by as much as 8 km/h (5 mph) near Lake Charles, LA (specifically, northeastern Calcasieu Parish and the eastern half of Beauregard Parish) (Applied Research Associates 2020). As the storm’s well-predicted track facilitated coordinated, multi-entity surface measurements of wind fields and storm surge, Laura is one of the best documented storm events and thus provides novel opportunities to understand the vulnerabilities underpinning losses and robustly verify and validate workflows intended to predict ensuing losses.

The Structural Extreme Events Reconnaissance (StEER) Network building performance assessments captured between 27 August and 12 September 2020 will serve as the ground truth observations for this validation exercise. Notably, the areas impacted by Laura were previously impacted by Hurricane Rita (2005), resulting in a sizable population of modern (post-IBC/IRC) single-family homes exposed to design-level winds. As such, the validation exercise focuses on wood 1-2 story single-family (WSF1-2) and 1-3 story multi-unit residential (WMUH1-3) construction subjected to wind hazards. In accordance with the regional simulation workflow introduced in Deierlein et al. (Deierlein et al. 2020), the augmented parcels of the Lake Charles, LA Inventory were assigned appropriate damage and loss functions from the Hazus Hurricane Damage and Loss Model (FEMA 2018b, 2021), implemented in the SimCenter's PELICUN application (Zsarnoczay 2019). For wind damage assessment, the HAZUS damage functions consist of tabular data for multiple damage states to describe their fragilities as functions of 3-second peak wind speed (PWS) at reference height (10 m) in open terrain. These tabular data are parsed in PELICUN to fit a continuous normal or lognormal cumulative density function for each fragility. For wind loss assessment, the HAZUS loss functions consist of tabular data mapping the peak wind speed to expected loss ratio. These tabular data are used by PELICUN to calibrate the expected loss ratio of individual damage states so that the damage and loss models are coupled for more realistic outcomes (Zsarnóczay and Deierlein 2020).

The regional simulation used in the following verification and validation exercises is orchestrated using the NHERI SimCenter's Regional Resilience Determination (R2D) Application (McKenna et al. 2021), driven by a surface-level wind field produced on 4 September 2020 by Applied Research Associates (ARA) and made available by National

Institute of Standards and Technology (NIST) on DesignSafe (Applied Research Associates 2020). The wind field incorporates storm track and central pressure data from the National Hurricane Center (NHC) through Forecast Advisory Number 33 and observations through 1200 UTC on 28 August 2020. The ARA windfield is first mapped to a rectangular grid with 0.01 to 0.02 degree intervals; the peak wind speed at the centroid of each building footprint is estimated by randomly sampling the PWS from its nearest four neighboring grid points. The hazard intensities defined by the PWS are then related to probabilities of damage and loss.

The geospatial distribution of estimated wind damage states and losses under Hurricane Laura are shown in Figure 10a,b, with Figure 10c plotting the cumulative distribution function (CDF) of the damage states. Hazus Damage States (DS) are defined as DS-0: no/very minor damage, DS-1: minor damage, DS-2: moderate damage, DS-3: severe damage and DS-4: destroyed (Vickery et al., 2006). Most residential buildings (75%) in the Lake Charles inventory were projected to have relatively minor to moderate wind damage (expected Damage State no greater than 2). Few residences are predicted to be in the extremes of the distribution: about 5% with damage no greater than DS-1 and another approximately 5% exceeding DS-3. The corresponding CDF of projected loss ratios is shown in Figure 10d, illustrating that about 20% of residences would expect a loss of no more than 10% of the total reconstruction cost, with about 10% of residences seeing a loss of half or more of the total reconstruction cost. All estimates are based on a *YearBuilt* predicted using NSI-trained machine-enabled techniques.

4.1 Verification Process

A two-step process was used for verification, with hand calculations of estimated losses for a subset of 98 randomly-sampled buildings in the inventory, followed by a parametric investigation. These hand calculation involve the manual assignment of the appropriate HAZUS building class based on the building attributes, followed by the manual selection of the corresponding damage fragilities and loss ratios from the HAZUS database that were described by best-fit curves in the SimCenter's Pelicun application (Zsarnóczay and Deierlein 2020). Peak wind speeds are determined using geolocation data from the ARA wind field contours. These peak wind speeds can then be substituted into the fitted damage and loss functions, for an overall verification that the loss estimatinon workflow is properly implemented. Hand-calculations simulated expected loss ratios for the sampled buildings showed excellent correlation with the simulated values, achieving a correlation coefficient of 0.9996. As a second verification step, parametric investigations on select case study buildings are used to heuristically examine the ruleset logic founded upon *YearBuilt*. Herein we present the parametric case study for a single-family house (1-story wood structure with a gable roof). The original building record is expanded to 51 different buildings by varying the YearBuilt between 1970 and 2020. For each building, the expected loss ratio is estimated using 50 realizations to consider the uncertainty from the rulesets assigning some attributes as random variables (e.g., the ruleset assigns use of secondary water resistance to buildings built after 2000 according to a 60% probability). The black curves in Figure 11 plot the individual realizations of expected loss ratio against different *YearBuilt* values. The red curve shows the mean value of 50 realizations for each *YearBuilt.* As expected, building performance generally improves following major code revisions. For example, as labeled by the yellow dashed line at 2000, the IRC 2000-2009 requires 8d nails (with spacing 6"/6" or 15.2 cm mm/15.2 cm) for sheathing thickness of 1" (25.4 mm) for basic wind speeds greater than 160 km/h (100 mph), which enhances the building performance (reducing the expected loss ratio). When this ultimate wind speed is increased to 130 mph (215 km/h) (just above the design wind speed) in a 2016 revision accepting the use of 6”/12” (15.2 cm/30.5 cm) spacing, a corresponding slight degradation in building performance is observed. This observation highlights the particular importance of nail spacing requirements for sheathing in reducing wind-induced losses for this class of construction.

4.2 Influence of Competing Data Sources

As demonstrated by the above verification process, YearBuilt is critical to assigning attributes within an Augmented Parcel approach reliant on time-evolving rulesets. Herein we examine the implications of assigning YearBuilt in data scarce environments using machine-enabled techniques trained against NSI and the commercial real estate platform, Zillow. Figure 12a illustrates the difference in estimated YearBuilt as predicted by Zillow- and NSI-trained models. The ensuing implications of using different sources of YearBuilt information to predict damage are visualized in Figure 12b. Note that differences in YearBuilt matter only when those differences shift the structure into not only a different code era in the ruleset logic, but to one with substantive changes either to the hazard description or the building’s load path or affected components, thus making the implications of errors in *YearBuilt* on the final loss estimation context dependent. Those types of substantive amendments can be on the scale of decades in less frequently-exposed locales like New Jersey, or even annually in more frequently-exposed locales like Louisiana. Figure 13a illustrates the subtle differences in the CDF for DS-2 and DS-3 between NSI- and Zillow-trained models, with Zillow tending to predict slightly higher damage states outside of the tails of the distribution where the transition to the modern code era takes place. The impact on damage ratings is not prominent in some of the areas with the largest differences in year built predictions, such as downtown Lake Charles (shown by dashed box in

Fig. 12b) or areas to the east to either side of I-10, where the construction is older and pre-dates the modern code era. However, some of the newer developments at the southernmost boundary of the municipality are in the modern code era, where differences in *YearBuilt* may translated into marked differences in ruleset-assigned attributes. This is illustrated by the previous validation case study and reinforced by Figure 13b, which shows the probability of a residence achieving the expected DS for four different *YearBuilt* ranges: Pre-1960, 1960-1979, 1980-1999, Post-2000. This underscores the challenges created both by the underreporting of YearBuilt values in this area, as well as the fact that the attributes necessary for loss estimation by Hazus are not routinely reported in inventory data nationwide. Finally, since the Zillow data used in this study was taken from Zillow Transaction and Assessment Database (ZTRAX), which has proprietary restrictions, the NSI-predicted *YearBuilt* is used for the loss assessments in the next section as this data is available to all readers without restriction.

4.3 StEER Validation Exercise

StEER used human visual inspections to rate damage on the Hazus-defined wind loss scale for a sampling of buildings in Lake Charles and surrounding areas (Roueche et al. 2021), referred to herein as *StEER Buildings.* Ninety-nine of these buildings correspond to footprints in the Lake Charles inventory, which offers an opportunity to validate the end result of this loss assessment workflow built upon augmented-parcel inventories. It is important to note that these damage assessments were not conducted according to StEER's standard protocols due to COVID-19 restrictions on travel. Instead, assessments were conducted virtually by humans remotely interrogating street-level panoramic images collected from car-mounted platforms (Roueche et al. 2021). Thus, StEER buildings offer a "ground truth" that is potentially less reliable in discerning some aspects of the damage than a traditional StEER mission with in-person, up-close forensic assessments. Also note that since rulesets from New Jersey are applied to assign attributes and are not consistent with the historical regulatory environment in Louisiana, the predicted damage states are also likely to be slightly lower, particularly for construction older than 2006 (the year Louisiana first adopted ICC model codes statewide). Finally, as also discussed in StEER's report (Roueche et al. 2020), there were low rates of compliance with shuttering requirements in the affected area. Thus it is likely that shutter use would be assigned by rulesets at a rate higher than actually observed in this hurricane, leading to lower levels of predicted damage than those observed in the field, as discussed shortly.

4.3.1 Roof Classifier

Since StEER data undergoes a data enrichment and quality control process that generates over 100 fields of component, material and geometric information, its records can be used to validate various aspects of the augmented parcel approach. For example, in order to further validate the roof classifier used to populate RoofShape attributes in the Lake Charles inventory, StEER Buildings were pre-processed to retain only those single-family homes tagged with roof shapes consistent with the three Hazus classes (N=56), discarding records labeled as "complex" according to StEER's more robust roof classification standards. The confusion matrix in Figure 14 affirms the effectiveness of the roof shape classifier in this validation exercise, recalling that perfect classification would have 1.0 scores along the diagonal. Comparison of this validation result (with 70% accuracy for hip and gable roofs) against the over 90% accuracy reported in Wang et al. (2021) underscores that contemporary roof shapes are far more complex than the three simplified geometries adopted by Hazus and even idealized in the initial training sets used to develop the SimCenter's roof classifier module. The limitations of simplifying roofs into one of three shapes not as common in contemporary construction forces humans classifying roofs, including StEER assessors, to attempt to subjectively force every roof into one of these categories, begging the larger question regarding the ability of our loss modeling capabilities to keep pace with modern construction trends. The adopted approach of using similitude measures to more objectively force classifications to the nearest simplified roof shape (gable, hip, flat) remains the most viable means to negotiate the very real disconnects between the simplified shapes adopted in conventional loss models and contemporary geometries in practice.

4.3.2 Damage Rating

Uncertainties inherent the hazard, building inventory and vulnerability models will affect the predicted level of damage. Unfortunately, the ground truth observations available from StEER do not include on-site wind speeds or reporting of all the building attributes employed by the adopted vulnerability model to allow isolation of the potential effects of these uncertainties on the overall damage rating. However, the implication of such uncertainties is explored herein for both hazard inensity and the building attribute most critical to the use of heuristic rulesets: *YearBuilt.* Assuming this building attribute follows a normal distribution with mean at the value assigned by machine-enabled techniques and standard deviation of 10 years, a sample of 100 *YearBuilt* values is generated for each of the 99 StEER buildings. This results in a distribution of simulated Damage States for that building (see example in Figure 15a). Figure 15b compares the resulting mean and 95th-percentile of these distributions of the simulated damage states to the StEER-observed damage state, where perfect agreement would cluster about the dashed diagonal line. Note that the simulated damage states are the result of three WSF1-2 attributes being assigned as random variables (see Table 2), which in addition to *YearBuilt* uncertainties, results in the scatter across simulated damage states. To aid in interpretation, an overall trend is visualized by the red points that define the bin average across the values at each damage state. The results suggest that while minor and moderate damage states are on average consistent with ground-truth observations, which is where the most observations cluster, the extremes characterized by fewer ground-truth observations suggest a bias toward minor damage for undamaged structures, with simulated damage rates plateauing around the moderate damage state even for severely damaged and collapsed buildings. The same type of uncertainty analysis is conducted for the peak wind speed, randomly sampling 100 PWS values from a normal distribution with mean set to the PWS specified by ARA for that building's location and a standard deviation of 20 mph. Analysis of the resulting mean and 95th-percentile of the distribution of these simulated damage states compared to the StEER-observed damage state in Figure 15c reiterates the same trend. Further note that changing the wind speed to explore the effect of uncertainties in the hazard intensity at a given site does not account for site-specific variations in the wind field itself, e.g., localized flow effects, which can have considerable impacts on the level of damage observed.

In an effort to understand potential sources of the simulation's unconservative bias for buildings with observed severe damage (DS-3) and destruction (DS-4), the rulesets used to generate the Lake Charles inventory were overridden to apply window protection as a random variable with compliance rates of 20% for all *YearBuilt* values, approximately half that observed in other coastal communities (Javeline and Kijewski-Correa 2019) and more consistent with StEER's anecdotal observations (Roueche et al. 2020). While this does slightly elevate the simulated damage values across all damage states, DS3 and DS4 are still underestimated (Fig. 15d). As damage states are driven by a number of attributes and site factors, including construction errors and material defects, the limited number of observations in DS-3 and DS-4 limits the ability to draw further conclusions. Still, access to StEER's field observations under design-level winds, acquired using component-level quantifications of damage that map to Hazus damage states, provides invaluable opportunities to validate and further improve loss modeling frameworks.

5.0 Conclusions

While computational simulation tools and high performance computing are rapidly advancing the collective potential to study the impact of hurricanes on communities and entire regions at unprecedented fidelity and granularity, their use in the study of real-world scenarios remains constrained by the availability and completeness of reliable parcel data. Even in the most data rich communities, exposed municipal data lacks a number of structural attributes necessary to predict damage and ensuing losses at the level of individual building footprints. This paper presents an augmented-parcel approach that defines a comprehensive data model inclusive of hazard and structural attributes necessary for Hazus-compatible risk assessments on a wide class of buildings under hurricane wind and flood hazards. The study further demonstrates how existing open municipal and third party data can be scraped to initially populate the required fields across a large-scale building inventory, assigning the remaining attributes using a series of machine learning modules and time-evolving rulesets grounded in local codes/standards, regional construction practices/norms, and human subjects data. These techniques are implemented within the regional hurricane loss assessment workflow of the NHERI SimCenter and available to the community as open software. Illustrative examples in a data-rich setting (Atlantic County, NJ) and a data-scarce municipality (Lake Charles, LA) demonstrate the workflow's replicability in digitizing large-scale building inventories, both of which are curated on DesignSafe.

The study's validations of computer vision-based modules to generate underreported building attributes underscores the importance of algorithms that are robust enough to reliably classify "in the wild" images scraped from platforms like Google Street View. Among these, the validation of an occupancy classifier further reiterated the need to go beyond semantically-inferred image labels for training data, ideally drawing data from local agencies where the targeted attribute is the focus of ongoing data gathering and quality assurance efforts. Improving performance further will require enabling nuanced classifications of the wide diversity of non-commercial construction, which can be challenging given the limited amounts of training data for occupancies that comprise a small fraction of the overall inventory. Validations of attached garage detectors similarly reinforced the need for representative local training data to recalibrate models to the architectural nuances in a given community, such as the carports. This reiterates that reliable regional inventory data is critical to the continued refinement of these classifiers.

The phased approach of augmenting available parcel data is in theory region-, hazard- and even loss model-agnostic, meaning that the same steps would be executed and tools engaged to mine required hazard, site and building attributes. Extensions outside of hurricane wind/flood within a Hazus framework would however require the development of a data model in Phase I that defines the relevant attributes for that hazard and/or adopted loss model. The population of that data model in Phase II would need to be accordingly adapted based on the data sources available in that region or for that hazard, as the case studies in New Jersey and Louisiana demonstrate. The techniques developed to efficiently scrape and parse such data are themselves universal. Developing the augmented parcel approach for a data scarce environ like Louisiana at minimum ensures Phase III is supported by a robust collection of available tools that can be deployed to assign under-reported data essential to the loss estimation in future applications. These tools may require recalibration in regions where construction practices, particularly aesthetic features, are dramatically different from those used in the development or the extension of these tools to new classes of features, e.g., vulnerabilities like soft stories (Yu et al. 2020). Finally, Phase IV would require some adjustment if translated to a new region with different code eras, design wind speeds, or load path requirements, as the discourse herein on New Jersey vs. Louisiana underscored. The availability of the rulesets used here in GitHub is intended to aid such adaptations. However, entirely new rulesets would be required for any changes in the hazard or loss estimation framework – though the adoption of Hazus herein addresses the most universal model in US practice. The SimCenter's released testbeds for earthquakes (https://simcenter.designsafe-ci.org/testbeds/) demonstrate such extensions of the methodology for other hazards, with its Pelicun application supporting loss assessments using Hazus and FEMA P-58 (Zsarnóczay and Deierlein 2020).

The study further underscored the criticality of accurate year built data for post-IBC/IRC construction eras, given the augmented parcel approach's reliance on time-evolving rulesets, in this case exploring the use of spatial inference to assign this critical field from limited observations in the National Structure Inventory and commercial real estate platforms like Zillow. Finally, a verification and validation exercise is conducted using StEER field observations collected in Lake Charles following the landfall of Hurricane Laura. The validations highlighted the incompatibilities between Hazus-simplified roof shapes and contemporary roof geometries, and the challenges it creates for classification by both human and machine agents. The SimCenter's workflow applying Hazus-based fragilities to the augmented-parcel inventories generated in this study were found to be consistent, on average, with ground-truth observations for the minor to moderate damage states that comprised the majority of field observations. Extreme damage states were characterized by fewer ground-truth observations, with simulations biasing toward minor damage for undamaged structures and plateauing at moderate damage even for severely damaged and collapsed buildings. This trend was maintained when investigating the uncertainty in hazard intensity, as well as the low rates of shutter compliance. This exercise in particular reiterates the importance of collecting rich post-disaster field observations to validate established loss-estimation frameworks and demonstrates the reuse potential of component-level quantifications of damage that map readily to damage states used by Hazus. Though beyond the scope of this study, root causes of inconsistencies revealed in this validation exercise will require further processing of street-level panoramic images captured by StEER. Such efforts should focus on expanding the limited number of structural assessments released in DesignSafe to increase the sample of severely damaged and collapsed buildings, as well as revisiting the forced classification of roofs into Hazus classes by using the classifier's similitude measures to establish thresholds defining roofs that are not accessible due to significant incompatibilities with basic roof geometries. Such efforts should leverage the inventory generated in this study and published on DesignSafe to identify regions reconstructed after Hurricane Rita to determine if damage states are more reliably estimated by an augmented parcel approach when minimum construction practices are enforced.

Data Availability Statement

Some or all data, models, or code generated or used during the study are available in a repository online in accordance with funder data retention policies. Specifically, inputs (inventories, rulesets, and hazard data), outputs (results), and supporting documentation for Lake Charles, LA are available in DesignSafe (https://doi.org/10.17603/ds2-83ca-r890). The pair of inventories and rulesets for Atlantic County, NJ are also available in DesignSafe (https://doi.org/10.17603/ds2-jpj2-zx14). See http://doi.org/10.5281/zenodo.5033626 to download the R2D application used to execute the regional simulations described herein. Full documentation for each of the inventories and R2D is available at https://nheri-simcenter.github.io/R2D-Documentation/index.html.

Acknowledgements

This material is based upon work supported by the National Science Foundation under Grant Nos. CMMI 1612843 & 2131111. Any opinions, findings, and conclusions or recommendations expressed in this material are those of the author(s) and do not necessarily reflect the views of the National Science Foundation. The authors acknowledge the larger collaborations with Sascha Hornauer, Wael Elhaddad, Greg Deierlein, and Andrew Kennedy on the regional testbeds for the NHERI SimCenter. The authors appreciate the special access to ZTRAX data provided by the University of California at Los Angeles (UCLA) and the group of Professor Ertugrul Taciroglu, access to NJDEP data and other inventory information by the New Jersey Department of Community Affairs (NJ DCA) and the office of Keith Henderson, and the assistance of Rachel Hamburger of the University of Notre Dame in assembling the literature review.

References

American Society of Civil Engineers. 2017. *Minimum Design Loads and Associated Criteria for*

Buildings and Other Structures. *Minim. Des. Loads Assoc. Criteria Build. Other Struct.* American Society of Civil Engineers.

Angeles, K., M. Lochhead, T. Kijewski-Correa, K. Zhong, and A. Zsarnoczay. 2021. "NHERI-SimCenter/AssetRepresentationRulesets: Version 1.0.0." https://doi.org/10.5281/ZENODO.5496056.

Applied Research Associates. 2020. "Hurricane Laura Rapid Response Windfield Estimate." *https://www.designsafe-ci.org/data/browser/public/designsafe.storage.community/Recon%20Portal/20d 20Hurricane%20Laura%20Cameron%20Louisiana%20USA*. Accessed March 12, 2022. https://www.designsafe-ci.org/data/browser/public/designsafe.storage.community/Recon Portal/20d 20Hurricane Laura Cameron Louisiana USA.

Applied Technology Council. n.d. "ATC Hazards by Location." Accessed March 12, 2022. https://hazards.atcouncil.org/.

Aravena Pelizari, P., C. Geiß, P. Aguirre, H. Santa María, Y. Merino Peña, and H. Taubenböck. 2021. "Automated building characterization for seismic risk assessment using street-level imagery and deep learning." *ISPRS J. Photogramm. Remote Sens.*, 180: 370–386. Elsevier. https://doi.org/10.1016/J.ISPRSJPRS.2021.07.004.

Center for Risk-Based Community Resilience Planning, v. 3. 5. . 2022. *IN-CORE Manual*.

Chen, L.-C., G. Papandreou, F. Schroff, and H. Adam. 2017. "Rethinking Atrous Convolution for Semantic Image Segmentation." *arXiv Prepr. arXiv1706.05587.*

Deierlein, G. G., and eds. Adam Zsarnóczay. 2021. *State of the Art in Computational Simulation for Natural Hazards Engineering*. https://doi.org/10.5281/ZENODO.4558106.

Deierlein, G. G., F. McKenna, A. Zsarnóczay, T. Kijewski-Correa, A. Kareem, W. Elhaddad, L. Lowes, M. J. Schoettler, and S. Govindjee. 2020. “A Cloud-Enabled Application Framework for Simulating Regional-Scale Impacts of Natural Hazards on the Built Environment.” *Front. Built Environ.*, 6. https://doi.org/10.3389/fbuil.2020.558706.

Department of the Treasury, S. of N. J. 2018. “MOD IV User Manual.” *https://www.state.nj.us/treasury/taxation/pdf/lpt/modIVmanual.pdf*.

Durnov, V. 2020. “1st Place Solution for xView2: Assess Building Damage Challenge.” GitHub. Accessed August 16, 2022. https://github.com/DIUx-xView/xView2_first_place.

Everingham, M., L. van Gool, C. K. I. Williams, J. Winn, and A. . Zisserman. 2012. “The PASCAL Visual Object Classes Challenge 2012 (VOC2012).” Accessed March 12, 2022. http://host.robots.ox.ac.uk/pascal/VOC/voc2012/index.html.

FEMA. 2018a. *HAZUS – Multi-hazard Loss Estimation Methodology 2.1, Flood Model Technical Manual*. Washington, DC: Federal Emergency Management Agency.

FEMA. 2018b. *HAZUS – Multi-hazard Loss Estimation Methodology 2.1, Hurricane Model Technical Manual*. Washington, DC: Federal Emergency Management Agency.

FEMA. 2021. *Hazus Hurricane Model Technical Manual Hazus 4.2 Service Pack 3*. Washington, DC: Federal Emergency Management Agency.

Fischler, M. A., and R. C. Bolles. 1981. "Graphics and Image Processing Random Sample Consensus: A Paradigm for Model Fitting with Applications to Image Analysis and Automated Cartography." *Commun. ACM*, (J. D. Foley, ed.), 24 (6): 381–395.

He, K., X. Zhang, S. Ren, and J. Sun. 2016. "Deep Residual Learning for Image Recognition." *Proc. IEEE Conf. Comput. Vis. pattern Recognit.*

International Building Code. 2018. *2018 International Building Code (IBC) | ICC Digital Codes*.

Jaiswal, K., and D. J. Wald. 2008. *Creating a Global Building Inventory for Earthquake Loss Assessment and Risk Management*.

Jaiswal, K., D. Wald, and K. Porter. 2010. "A Global Building Inventory for Earthquake Loss Estimation and Risk Management." *Earthq. Spectra*, 26 (3): 731–748. https://doi.org/10.1193/1.3450316.

Javeline, D., and T. Kijewski-Correa. 2019. "Coastal homeowners in a changing climate." *Clim. Change*, 152 (2): 259–274. https://doi.org/10.1007/s10584-018-2257-4.

Kijewski-Correa, T., B. Cetiner, K. Zhong, C. Wang, A. Zsarnóczay, M. Lochhead, F. McKenna, and G. Deierlein. 2022. *SimCenter Hurricane Testbed: Atlantic County, NJ*. DesignSafe, https://doi.org/10.17603/ds2-83ca-r890.

Kijewski-Correa, T., A. Taflanidis, C. Vardeman, J. Sweet, J. Zhang, R. Snaiki, T. Wu, Z. Silver, and A. Kennedy. 2020. "Geospatial Environments for Hurricane Risk Assessment: Applications to Situational Awareness and Resilience Planning in New Jersey." *Front. Built Environ.*, 6. https://doi.org/10.3389/fbuil.2020.549106.

Kingma, D. P., and J. Lei Ba. 2014. *ADAM:* A method for stochastic optimization. arXiv preprint 811 arXiv:1412.6980.

Lin, T.-Y., M. Maire, S. Belongie, J. Hays, P. Perona, D. Ramanan, P. Dollár, and C. L. Zitnick. 2014. *LNCS 8693 - Microsoft COCO: Common Objects in Context*. In Proc., *European Conf. on computer vision,* 740-755. Springer, Cham

McKenna, F., S. Gavrilovic, A. Zsarnoczay, K. Zhong, and W. Elhaddad. 2021. "NHERI-SimCenter/R2DTool: Version 1.1.0." https://doi.org/10.5281/ZENODO.5033626.

Microsoft. 2021. "GitHub - microsoft/USBuildingFootprints: Computer generated building footprints for the United States." Accessed March 12, 2022. https://github.com/microsoft/USBuildingFootprints.

Nawari, N. O., and S. Ravindran. 2019. "buildings Blockchain and Building Information Modeling (BIM): Review and Applications in Post-Disaster Recovery." *Buildings*, 9: 149. https://doi.org/10.3390/buildings9060149.

New Jersey Department of Environmental Protection. 2019. *NJDEP Building Footprints: Final Report*. Trenton, NJ.

New Jersey Geographic Information Network. 2021. "Parcels and MOD-IV of Atlantic County, New Jersey." NJGIN Open Data, https://njogis-newjersey.opendata.arcgis.com/documents/newjersey::parcels-and-mod-iv-of-atlantic-828 county-nj-shp-download/about.

New Jersey Office of Emergency Management. 2014. *State of New Jersey 2014 State Hazard*

Mitigation Plan. Trenton, NJ.

Park, H., D. T. Cox, and A. R. Barbosa. 2017. “Comparison of Inundation Depth and Momentum Flux based Fragilities for Probabilistic Tsunami Damage Assessment and Uncertainty Analysis.” *Coast. Eng.*, 10–26.

Pinelli, J.-P., J. Da Cruz, K. Gurley, P.-T. Andres Santiago, M. Baradaranshoraka, S. Cocke, and D. Shin. 2020. “Uncertainty Reduction Through Data Management in the Development, Validation, Calibration, and Operation of a Hurricane Vulnerability Model.” *Int. J. Disaster Risk Sci.*, 11: 790–806. https://doi.org/10.1007/s13753-020-00316-4.

Roohi, M., J. W. van de Lindt, N. Rosenheim, Y. Hu, and H. Cutler. 2021. “Implication of building inventory accuracy on physical and socio-economic resilience metrics for informed decision-making in natural hazards.” *Struct. Infrastruct. Eng.*, 17 (4): 534–554. Taylor & Francis. https://doi.org/10.1080/15732479.2020.1845753.

Rosenheim, N., R. Guidotti, P. Gardoni, and W. G. Peacock. 2021. “Integration of detailed household and housing unit characteristic data with critical infrastructure for post-hazard resilience modeling.” *Sustain. Resilient Infrastruct.*, 6 (6): 385–401. Taylor & Francis. https://doi.org/10.1080/23789689.2019.1681821.

Roueche, D., S. Kameshwar, J. Marshall, N. Mashrur, T. Kijewski-Correa, K. Gurley, I. Afanasyeva, G. Brasic, J. Cleary, D. Golovichev, O. Lafontaine, F. Lombardo, L. Micheli, B. Phillips, D. Prevatt, I. Robertson, J. Schroeder, D. Smith, S. Strader, M. Wilson, K. Ambrose, H. Rawajfih, and L. Rodriguez. 2020. *Hybrid Preliminary Virtual Reconnaissance Report-Early Access Reconnaissance Report (PVRR-EARR) in StEER -*

Hurricane Laura. DesignSafe-CI. https://doi.org/10.17603/ds2-ng93-se16.

Roueche, D., S. Kameshwar, M. Vorce, T. Kijewski-Correa, J. Marshall, N. Mashrur, K. Ambrose, C. Brown, O. Childress, D. Fox, K. Morris, H. Rawajfih, and L. Rodriguez. 2021. *Field Assessment Structural Teams: FAST-1, FAST-2, FAST-3 in StEER-Hurricane Laura*. DesignSafe. https://doi.org/10.17603/ds2-dha4-g845.

Shultz, S. 2017. "Accuracy of HAZUS General Building Stock Data." *Nat. Hazards Rev.*, 18 (4). https://doi.org/10.1061/(ASCE)NH.1527-6996.0000258.

SimCenter. 2022. "Building Recognition using AI at Large-Scale, NHERI SimCenter Documentation." *https://nheri-simcenter.github.io/BRAILS-Documentation/index.html*.

Stewart, R., M. Urban, S. Duchscherer, J. Kaufman, A. Morton, G. Thakur, J. Piburn, J. Moehl, and R. Stewart stewartrn. 2016. "A Bayesian machine learning model for estimating building occupancy from open source data." 81: 1929–1956. https://doi.org/10.1007/s11069-016-2164-9.

Tan, M., R. Pang, and Q. V. Le. 2020. "EfficientDet: Scalable and Efficient Object Detection." *Proc. IEEE/CVF Conf. Comput. Vis. pattern Recognit.*, 10781–10790.

Waddell, P. 2002. "UrbanSim: Modeling Urban Development for Land Use, Transportation, and Environmental Planning." *J. Am. Plan. Assoc.*, 68 (3): 297–314. Paul Waddell. https://doi.org/10.1080/01944360208976274.

Wang, C., S. Govindjee, F. McKenna, S. Yu, M. Schoettler, and K. Law. 2021a. "SimCenter Labeled Building Facades from Street View | DesignSafe-CI." DesignSafe.

https://doi.org/10.17603/ds2-z5ra-2260.

Wang, C., S. Hornauer, B. Cetiner, Y. Guo, F. McKenna, Q. Yu, S. X. Yu, E. Taciroglu, and K. H. Law. 2021b. "NHERI-SimCenter/BRAILS: Release v2.0.0." https://doi.org/10.5281/ZENODO.4570554.

Wang, C., K. Zhong, B. Cetiner, T. Kijewski-Correa, A. Zsarnóczay, F. McKenna, and G. Deierlein. 2021c. "SimCenter Hurricane Testbed: Lake Charles, LA." DesignSafe-CI. https://doi.org/10.17603/ds2-jpj2-zx14.

Yu, Q., C. Wang, B. Cetiner, S. X. Yu, F. Mckenna, E. Taciroglu, and K. H. Law. 2019. "Building Information Modeling and Classification by Visual Learning At A City Scale." https://doi.org/10.5281/zenodo.3996808.

Yu, Q., C. Wang, F. McKenna, S. X. Yu, E. Taciroglu, B. Cetiner, and K. H. Law. 2020. "Rapid visual screening of soft-story buildings from street view images using deep learning classification." *Earthq. Eng. Eng.*, 19 (4). https://doi.org/10.1007/s11803-020-0598-2.

Zhou, Y., H. Qi, and Y. Ma. 2019. "End-to-End Wireframe Parsing." *Proc. IEEE/CVF Int. Conf. Comput. Vis.* , 962–971.

Zsarnoczay, A. 2019. "NHERI-SimCenter/pelicun: pelicun v2.0.0." Accessed March 12, 2022. https://zenodo.org/record/3491100.

Zsarnóczay, A., A.-M. Deierlein, Gregory G. Williams, Caroline J. Kijewski-Correa, Tracy L. Esnard, L. Lowes, and L. Johnson. 2022. "Community Perspectives on Simulation and Data Needs for the Study of Natural Hazard Impacts and Recovery." *Nat. Hazards Rev.*, In Press.

Zsarnóczay, A., and G. G. Deierlein. 2020. “PELICUN - A Computational Framework for Estimating Damage , Loss and Community Resilience.” *17th World Conf. Earthq. Eng.*, 1–12. Sendai, Japan.

Figure Captions

Figure 1. Flow chart depicting the four sequential phases of the augmented parcel approach.

Figure 2. Sample images of the floor detection model (each detection is indicated by a green bounding box). The percentage value shown on the top right corner of a bounding box indicates model confidence level associated with that prediction.

Figure 3. Confusion matrices for the NumberOfStories predictor for (a) in the wild and (b) cleaned images.

Figure 4. Validation of predicted *OccupancyClass* using (a) OpenStreetMap and (b) NJDEP.

Figure 5. SURF-predicted YearBuilt based on NSI data compared to "ground truth" scraped from Zillow real estate listings in Lake Charles, LA displayed as (a) scatter plot and (b) histogram. Dashed lines denote +/- 10-years.

Figure 6. Examples of garage detection model showing successful identification of attached garages.

Figure 7. Confusion matrices for the garage predictor for validation sets from (a) New Jersey and California and (b) Lake Charles, LA.

Figure 8. Geospatial visualization of occupancy for New Jersey inventories with summaries of: occupancy class, year built and number of stories. Inset maps show progressive zoom-in on Atlantic City and surrounding municipalities.

Figure 9. Geospatial visualization of year built for the Lake Charles, LA building inventory with summaries of: (a) number of stories, (b) occupancy class, and (c) year built. Inset box identifies two clusters of buildings used in subsequent validations.

Figure 10. Geospatial distribution of (a) damage states and (b) loss ratios for Lake Charles inventory with cumulative distribution functions for (c) damage state and (d) expected loss ratio for Hurricane Laura Validation Exercise.

Figure 11. Parametric verification of expected loss ratio as a function of *YearBuilt* for case study single family home in Lake Charles inventory.

Figure 12. Difference between Zillow and NSI predicted (a) YearBuilt and (b) Damage State for Lake Charles inventory.

Figure 13. (a) Probability of meeting or exceeding DS-2 and DS-3 and (b) probability of meeting or exceeding the expected damage state using NSI-trained results based on YearBuilt for Lake Charles inventory.

Figure 14. Validation of BRAILS-predicted roof shapes to roof shapes labeled by StEER assessors in Lake Charles metro area.

Figure 15. (a) Damage State distribution compared to median damage state of StEER Buildings, (b) influence of uncertainty in YearBuilt on simulated Damage States, (c) influence of uncertainty in Peak Wind Speed on simulated Damage States, (d) influence of uncertainty in YearBuilt on simulated Damage States for low shuttering compliance. Red trend line shows the average of the displayed bins.

Table 1. Distribution of occupancies and label sources for occupancy classifier (N=15,743)

	RES 1	RES3	COM
OpenStreetMap	2,868	2,207	2,418
NJDEP	4,999	2,867	386
Total	**7,868**	**5,074**	**2,804**

Table 2. Methodology adopted for ruleset development

Attribute	Description	CS	PN	HS	RV	DA
Structural Attributes: Wind						
RoofSystem	Underlying roof structure		X			
SecondaryWaterResistance	Secondary Water Resistance (SWR)	X		X	X	
RoofCover	Roof cover material		X			
RoofQuality	Roof cover quality		X			
RoofDeckAttachmentW	Wood Roof Deck Attachment (RDA)	X			X	
RDA-OWSJ	OWSJ Roof Deck Attachment (RDA)	X				
RoofToWallConnection	Roof to Wall Connection (R2WC)	X				
Shutters	Window opening protection	X		X	X	
AttachedGarage	Presence of attached garage					X
MasonryReinforcing	Presence of reinforcement in masonry walls	*X*				
OWSJ-r	Property of open web steel joist (OWSJ)				X	
RoofDeckAttachmentM	Defines metal roof deck attachment (RDA)		X			
RoofDeckAge	roof deck age		X			
UnitClass	number of units in strip mall					X
JoistSpace	joist spacing for multi-unit strip malls		X			
WindDebris	likely sources of wind debris		X			
WindowAreaRatio	window to wall ratio (WWR)		X			X
TieDowns	Foundation attachment (mobile homes)	X			X	
Structural Attributes: Flood						
FloodType	Flood zone type					X
FirstFloorElev	First floor elevation, defined by Hazus					X
PostFIRM	FIRM applicability	X				
NumberofStoriesH	Hazus-defined number of stores					X
BasementType	Hazus basement classification					X
OccupancyType	Hazus occupancy type					X

Notes: Assigned by CS: codes/standards, PN: local construction practices/norms, HS: human-subjects surveys, RV: random variable, DA: direct assignment on other fields.

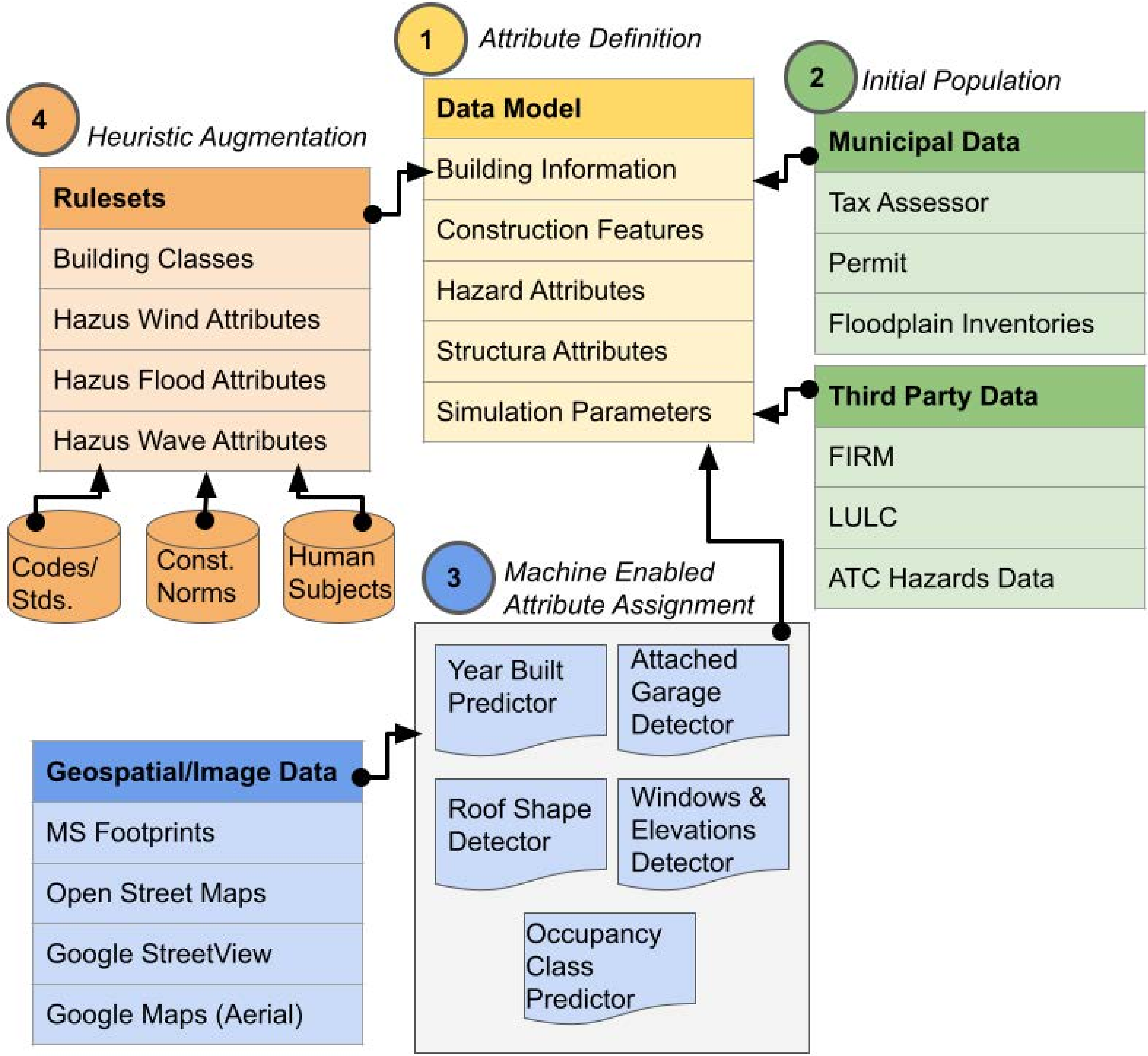
1
Attribute Definition
Data Model
Building Information
Construction Features
Hazard Attributes
Structura Attributes
Simulation Parameters
2
Initial Population
Municipal Data
Tax Assessor
Permit
Floodplain Inventories
Third Party Data
FIRM
LULC
ATC Hazards Data
4
Heuristic Augmentation
Rulesets
Building Classes
Hazus Wind Attributes
Hazus Flood Attributes
Hazus Wave Attributes
Codes/ Stds.
Const. Norms
Human Subjects
3
Machine Enabled Attribute Assignment
Year Built Predictor
Attached Garage Detector
Roof Shape Detector
Windows & Elevations Detector
Occupancy Class Predictor
Geospatial/Image Data
MS Footprints
Open Street Maps
Google StreetView
Google Maps (Aerial)


floor: 88%
floor: 84%

floor: 63%
floor: 39%
floor: 65%
floor: 37%
floor: 58%
floor: 64%

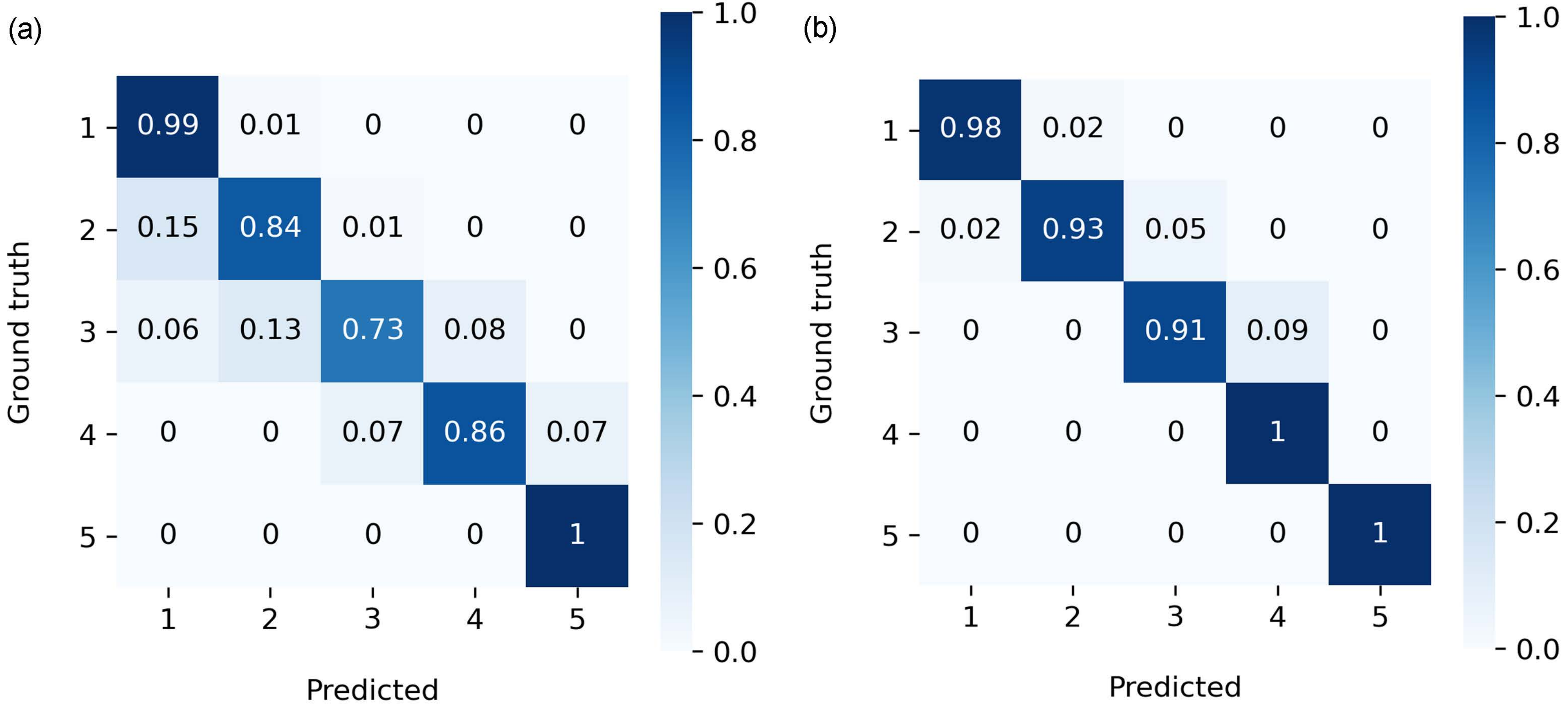
(a)
Ground truth
Predicted
1 2 3 4 5
0.99 0.01 0 0 0
0.15 0.84 0.01 0 0
0.06 0.13 0.73 0.08 0
0 0 0.07 0.86 0.07
0 0 0 0 1
0.0 0.2 0.4 0.6 0.8 1.0
(b)
Ground truth
Predicted
1 2 3 4 5
0.98 0.02 0 0 0
0.02 0.93 0.05 0 0
0 0 0.91 0.09 0
0 0 0 1 0
0 0 0 0 1
0.0 0.2 0.4 0.6 0.8 1.0

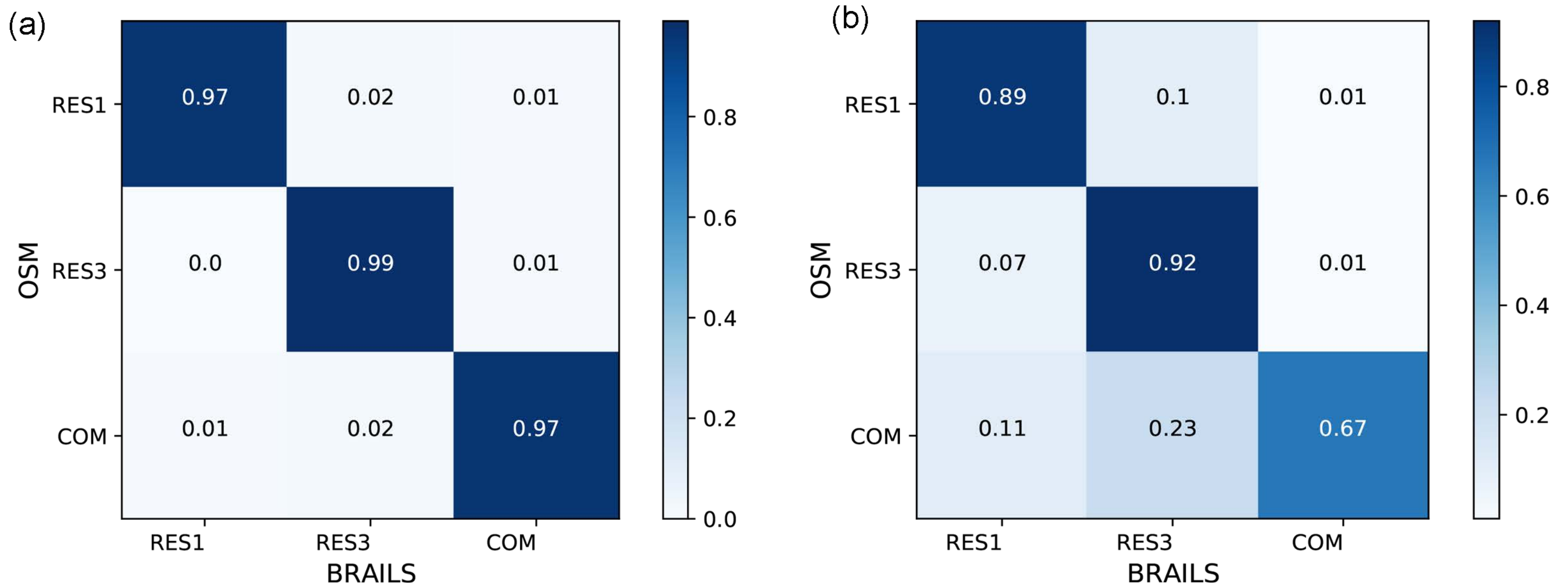

(a)
RES1
RES3
COM
OSM
BRAILS
0.97
0.02
0.01
0.0
0.99
0.01
0.01
0.02
0.97
0.0
0.2
0.4
0.6
0.8
(b)
0.89
0.1
0.01
0.07
0.92
0.01
0.11
0.23
0.67

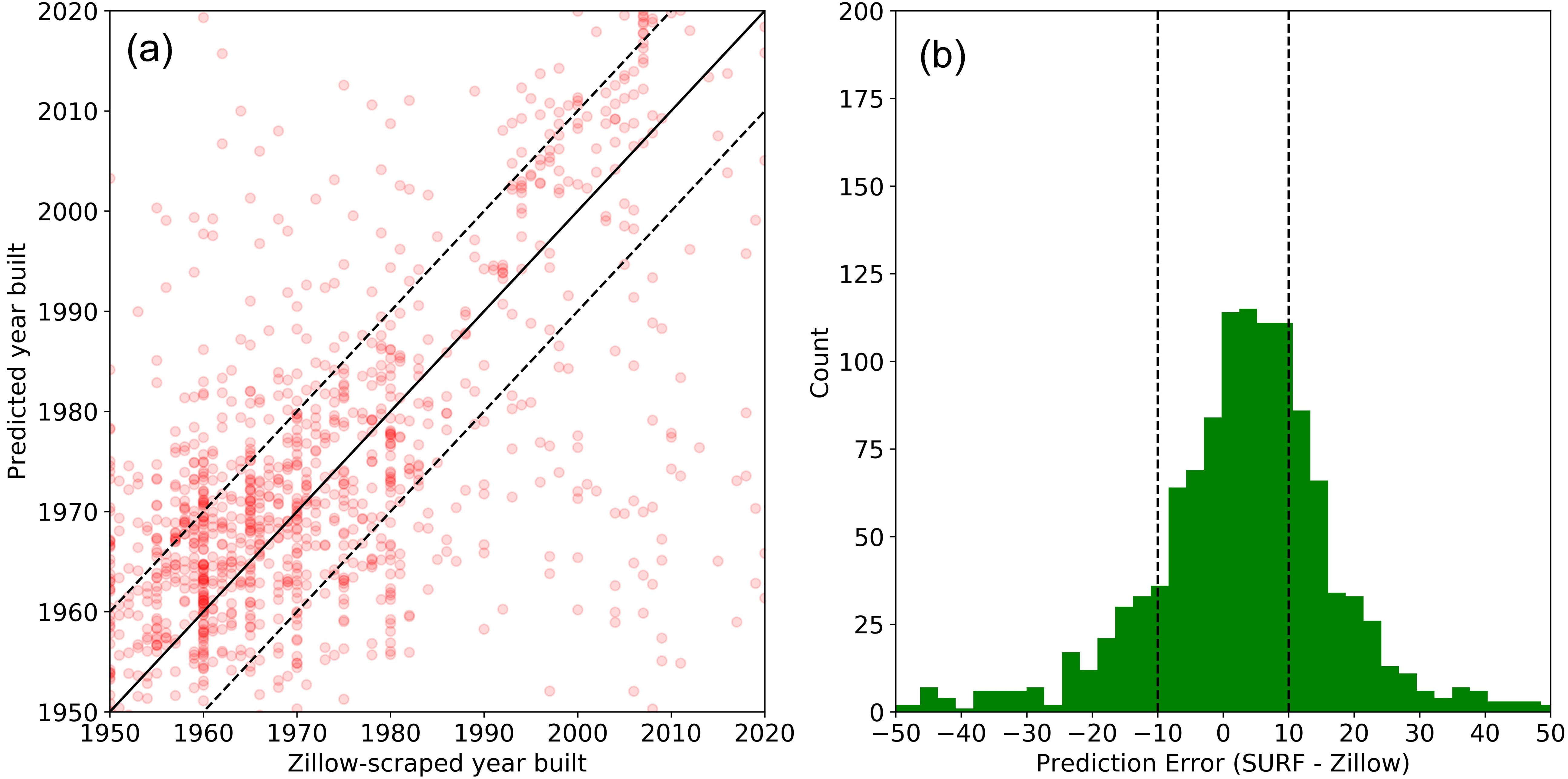

(a)
Predicted year built
Zillow-scraped year built
1950
1960
1970
1980
1990
2000
2010
2020
(b)
Count
Prediction Error (SURF - Zillow)
0
25
50
75
100
125
150
175
200
−50
−40
−30
−20
−10
0
10
20
30
40
50


age: 41%
garage: 51%
garage: 59%
garage: 67%

garage: 59%
garage: 84%

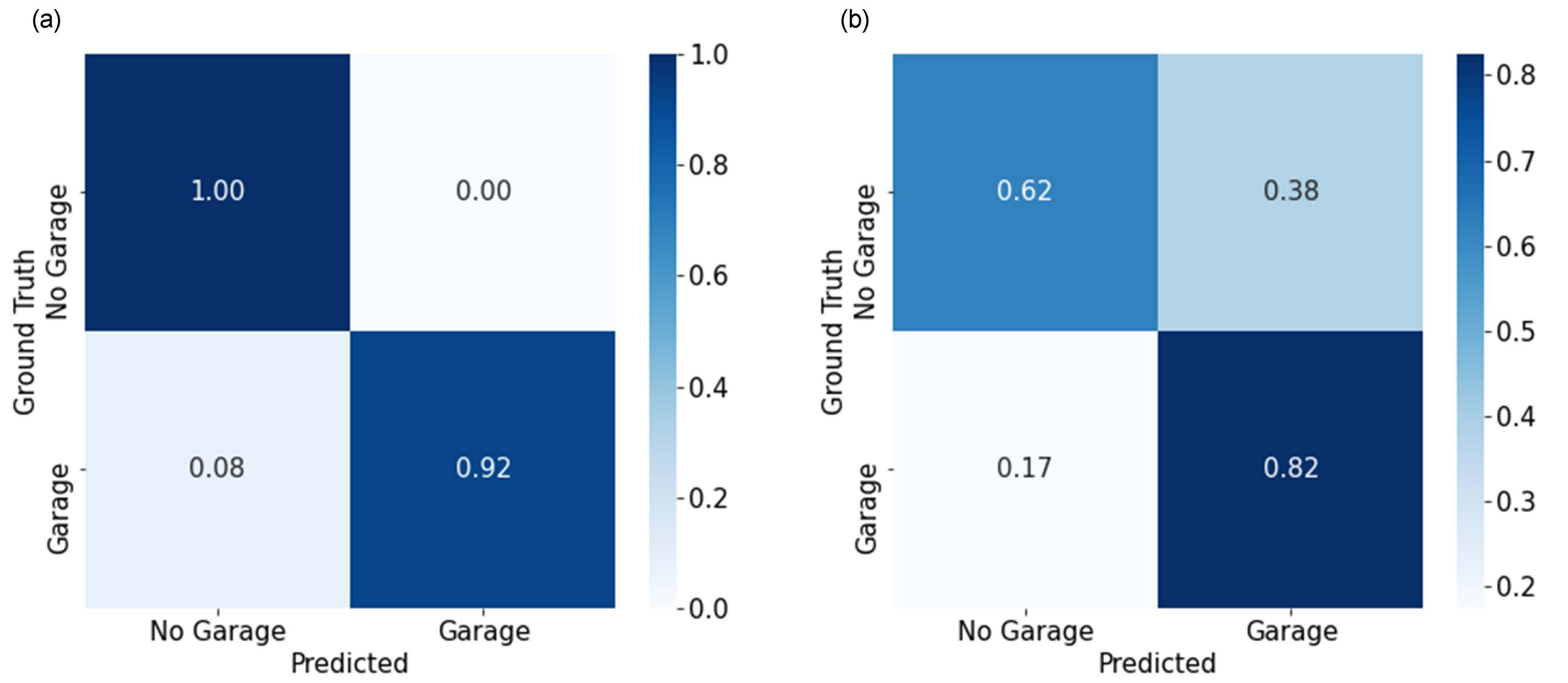
(a)
(b)
Ground Truth
No Garage
Garage
Predicted
1.00
0.00
0.08
0.92
0.62
0.38
0.17
0.82
1.0
0.8
0.6
0.4
0.2
0.0
0.7
0.5
0.3

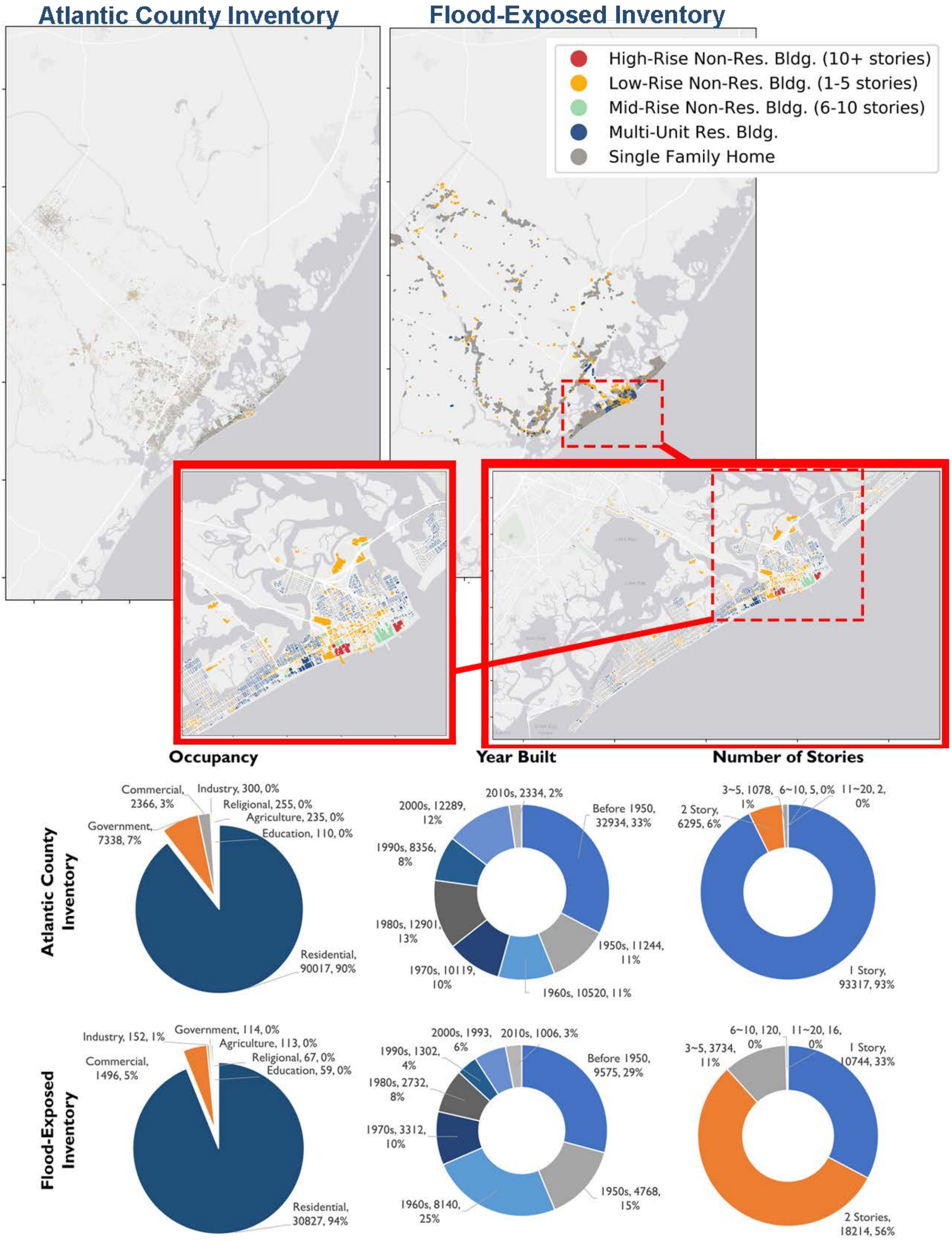

Atlantic County Inventory
Flood-Exposed Inventory
High-Rise Non-Res. Bldg. (10+ stories)
Low-Rise Non-Res. Bldg. (1-5 stories)
Mid-Rise Non-Res. Bldg. (6-10 stories)
Multi-Unit Res. Bldg.
Single Family Home
Occupancy
Year Built
Number of Stories
Atlantic County Inventory
Commercial, 2366, 3%
Industry, 300, 0%
Religional, 255, 0%
Agriculture, 235, 0%
Education, 110, 0%
Government, 7338, 7%
Residential, 90017, 90%
2010s, 2334, 2%
2000s, 12289, 12%
Before 1950, 32934, 33%
1990s, 8356, 8%
1980s, 12901, 13%
1970s, 10119, 10%
1960s, 10520, 11%
1950s, 11244, 11%
3~5, 1078, 1%
6~10, 5, 0%
11~20, 2, 0%
2 Story, 6295, 6%
1 Story, 93317, 93%
Flood-Exposed Inventory
Government, 114, 0%
Industry, 152, 1%
Agriculture, 113, 0%
Commercial, 1496, 5%
Religional, 67, 0%
Education, 59, 0%
Residential, 30827, 94%
2000s, 1993, 6%
2010s, 1006, 3%
1990s, 1302, 4%
Before 1950, 9575, 29%
1980s, 2732, 8%
1970s, 3312, 10%
1960s, 8140, 25%
1950s, 4768, 15%
6~10, 120, 0%
11~20, 16, 0%
3~5, 3734, 11%
1 Story, 10744, 33%
2 Stories, 18214, 56%

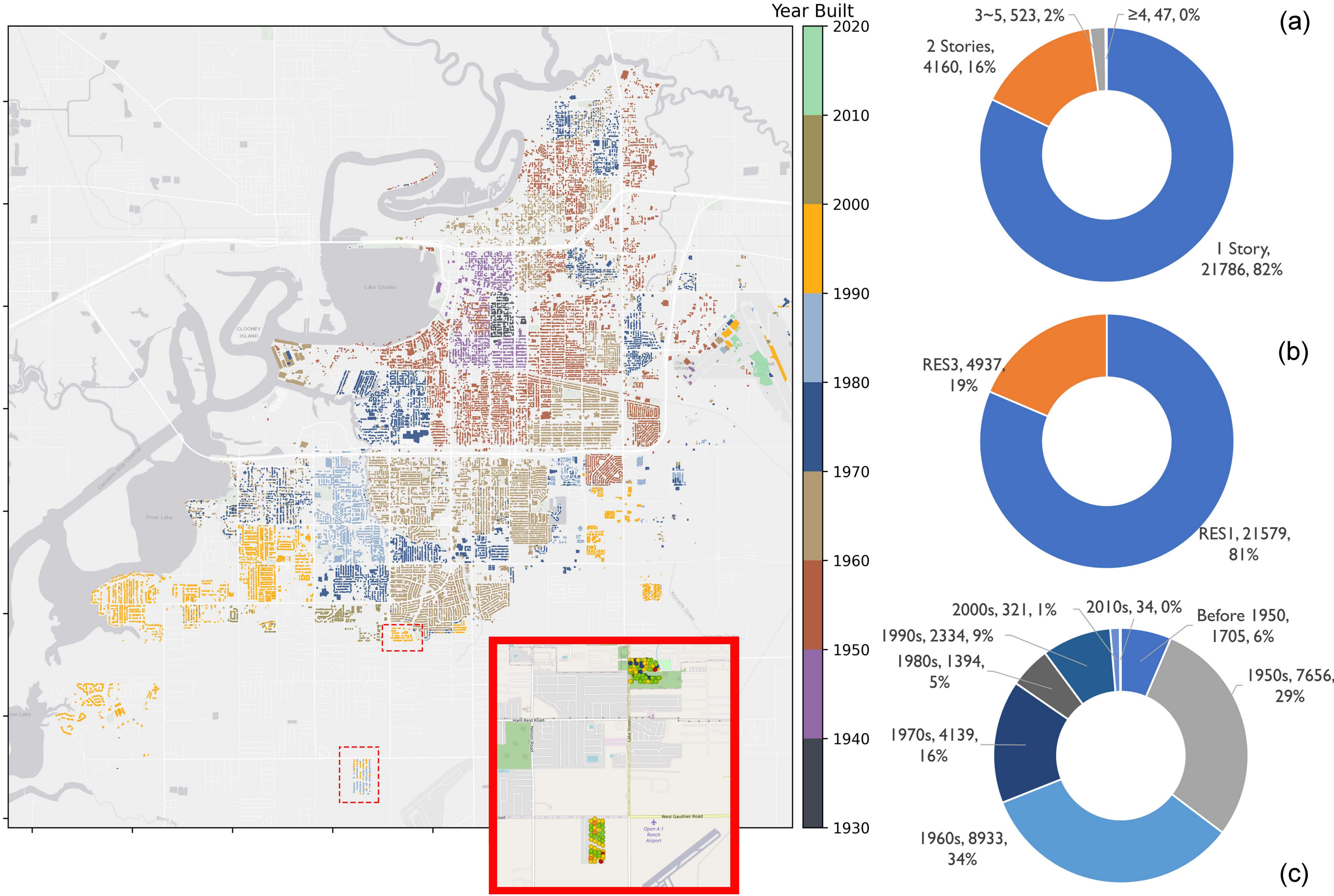

Year Built
2020
2010
2000
1990
1980
1970
1960
1950
1940
1930
Lake Charles
CLOONEY ISLAND
Prien Lake
Ham Reid Road
West Gauthier Road
Open A-1 Ranch Airport
(a)
3~5, 523, 2%
≥4, 47, 0%
2 Stories, 4160, 16%
1 Story, 21786, 82%
(b)
RES3, 4937, 19%
RES1, 21579, 81%
(c)
2000s, 321, 1%
2010s, 34, 0%
Before 1950, 1705, 6%
1990s, 2334, 9%
1980s, 1394, 5%
1950s, 7656, 29%
1970s, 4139, 16%
1960s, 8933, 34%

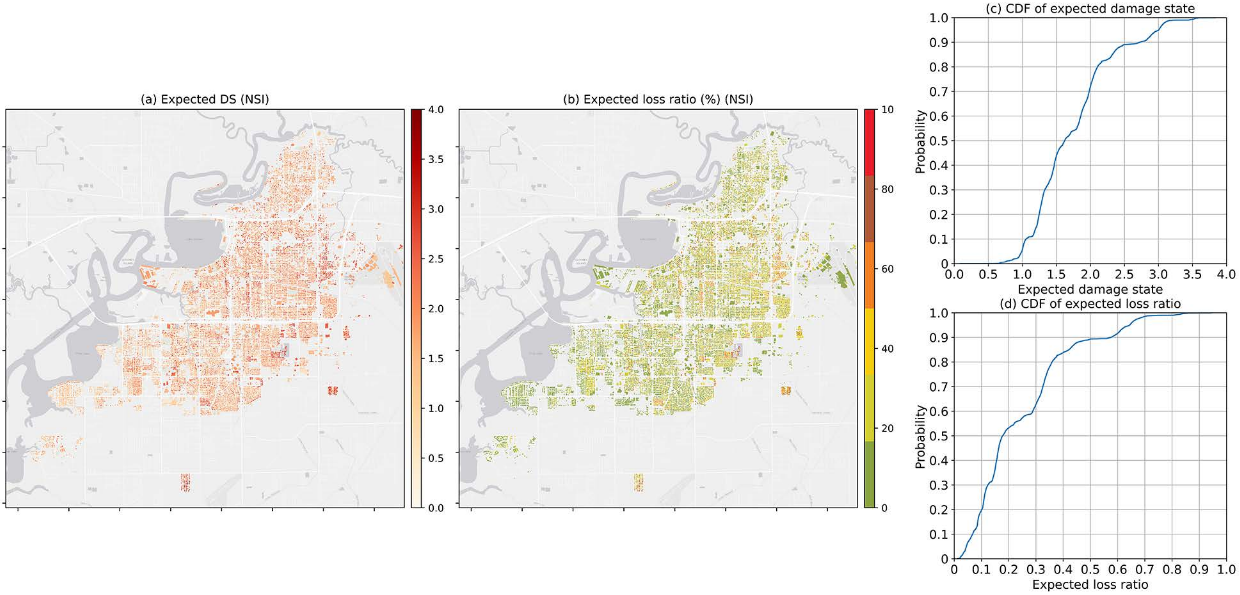

(a) Expected DS (NSI)
0.0
0.5
1.0
1.5
2.0
2.5
3.0
3.5
4.0
(b) Expected loss ratio (%) (NSI)
0
20
40
60
80
10
(c) CDF of expected damage state
Probability
Expected damage state
0.0 0.5 1.0 1.5 2.0 2.5 3.0 3.5 4.0
0 0.1 0.2 0.3 0.4 0.5 0.6 0.7 0.8 0.9 1.0
(d) CDF of expected loss ratio
Probability
Expected loss ratio
0 0.1 0.2 0.3 0.4 0.5 0.6 0.7 0.8 0.9 1.0

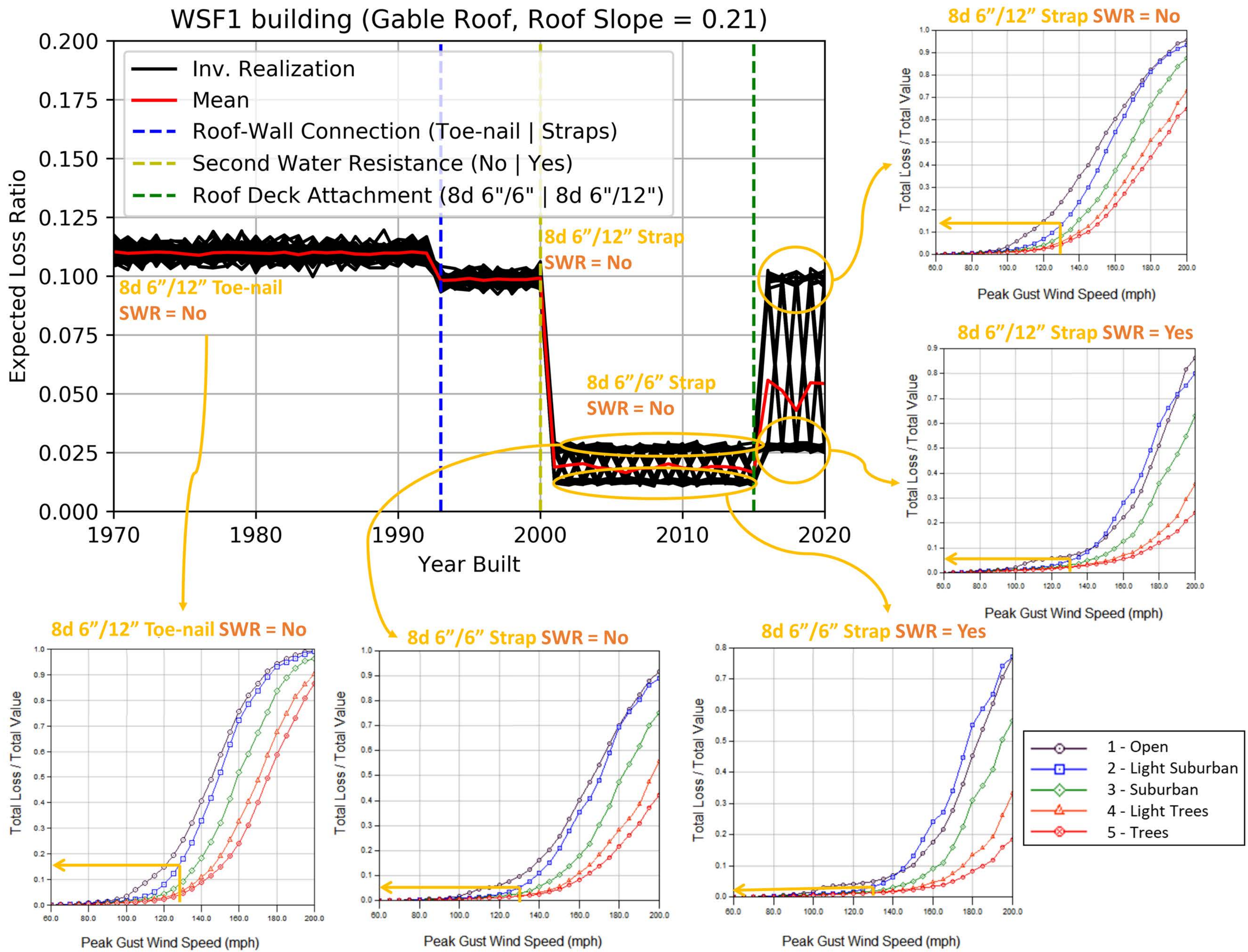
WSF1 building (Gable Roof, Roof Slope = 0.21)
Inv. Realization
Mean
Roof-Wall Connection (Toe-nail | Straps)
Second Water Resistance (No | Yes)
Roof Deck Attachment (8d 6"/6" | 8d 6"/12")
Expected Loss Ratio
Year Built
8d 6"/12" Toe-nail
SWR = No
8d 6"/12" Strap
SWR = No
8d 6"/6" Strap
SWR = No
8d 6"/12" Strap SWR = No
8d 6"/12" Strap SWR = Yes
8d 6"/12" Toe-nail SWR = No
8d 6"/6" Strap SWR = No
8d 6"/6" Strap SWR = Yes
Total Loss / Total Value
Peak Gust Wind Speed (mph)
1 - Open
2 - Light Suburban
3 - Suburban
4 - Light Trees
5 - Trees

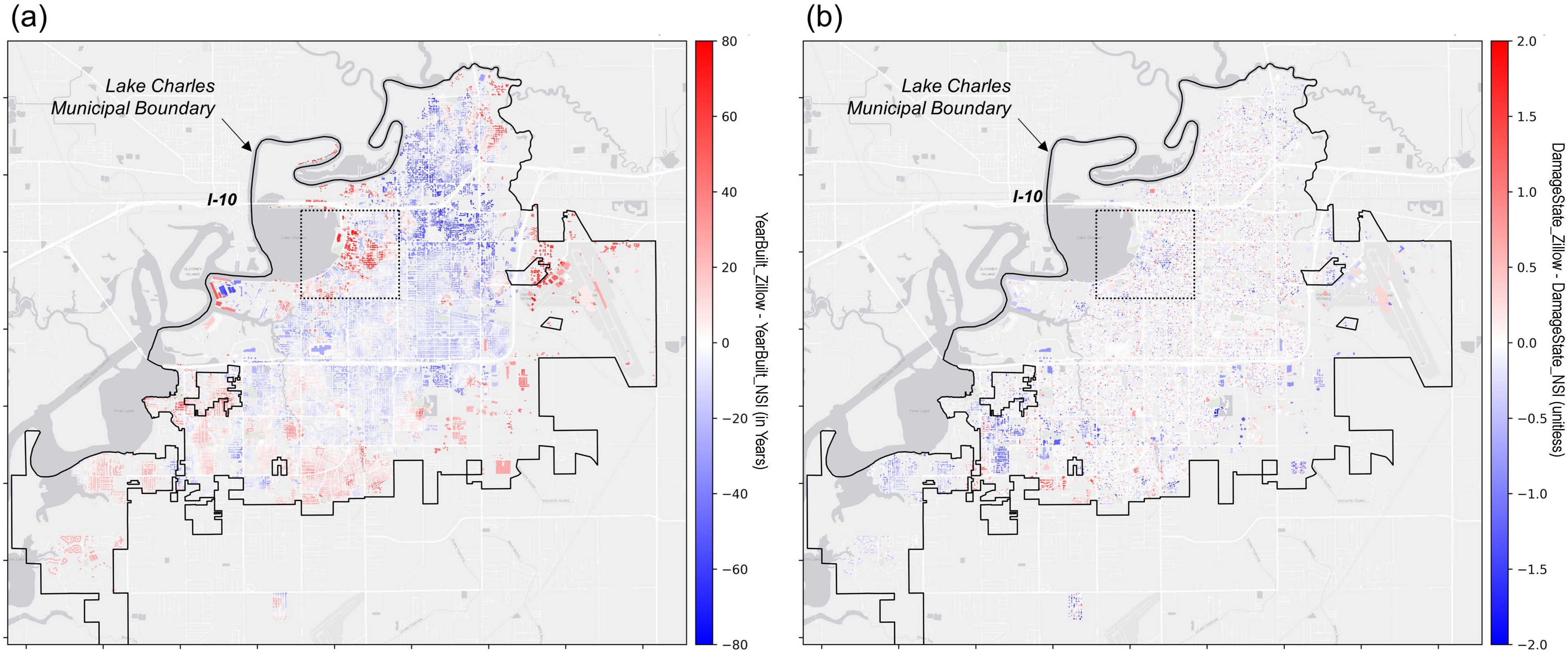

(a)
Lake Charles
Municipal Boundary
I-10
80
60
40
20
0
−20
−40
−60
−80
YearBuilt_Zillow - YearBuilt_NSI (in Years)
(b)
Lake Charles
Municipal Boundary
I-10
2.0
1.5
1.0
0.5
0.0
−0.5
−1.0
−1.5
−2.0
DamageState_Zillow - DamageState_NSI (unitless)

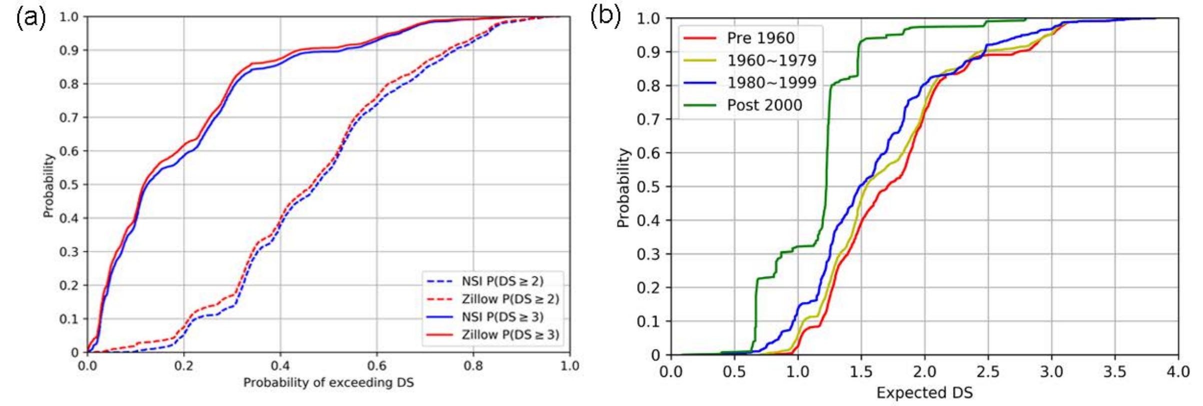
(a)
Probability
Probability of exceeding DS
NSI P(DS ≥ 2)
Zillow P(DS ≥ 2)
NSI P(DS ≥ 3)
Zillow P(DS ≥ 3)
(b)
Probability
Expected DS
Pre 1960
1960~1979
1980~1999
Post 2000

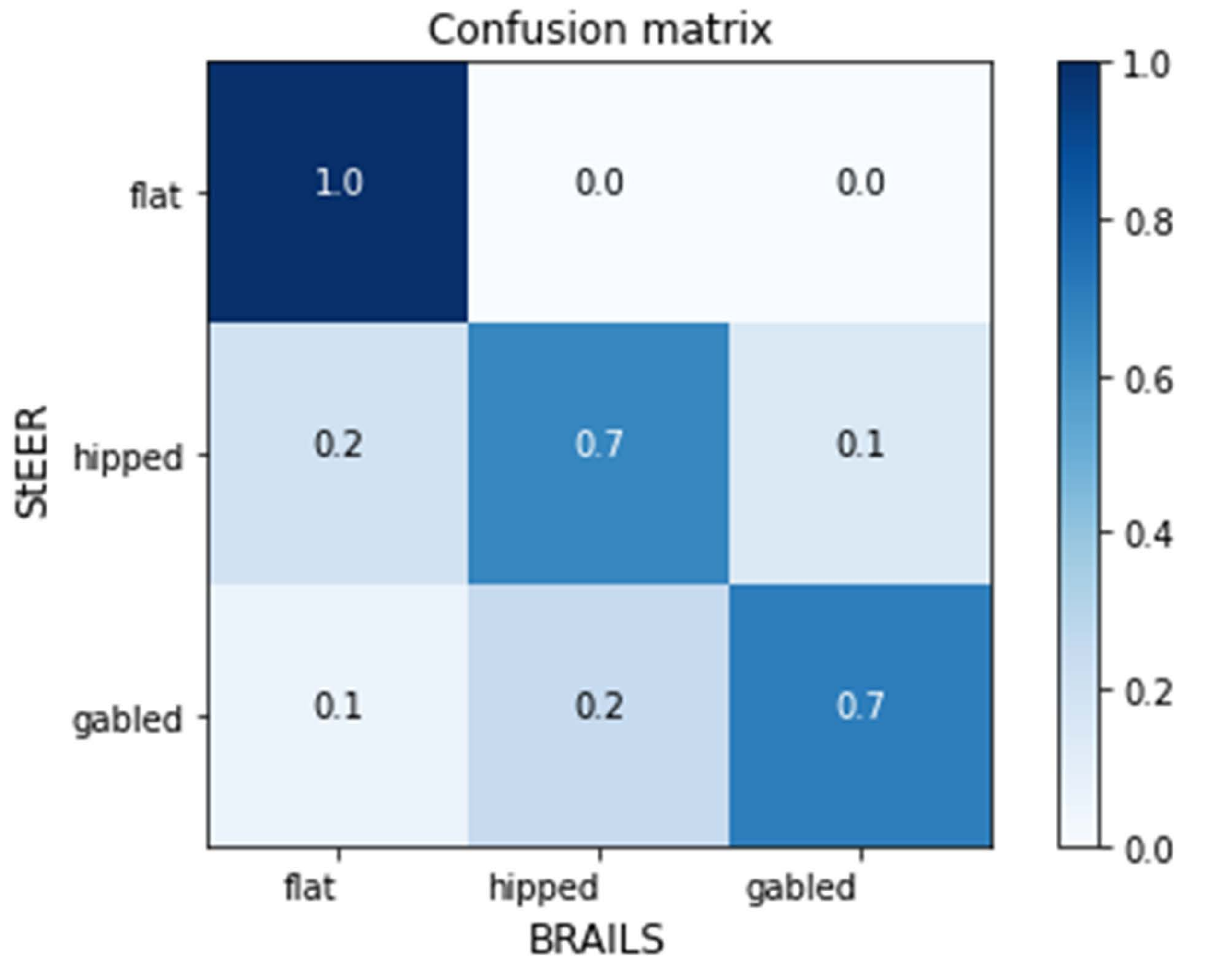
Confusion matrix
flat
hipped
gabled
StEER
1.0
0.0
0.0
0.2
0.7
0.1
0.1
0.2
0.7
flat
hipped
gabled
BRAILS
1.0
0.8
0.6
0.4
0.2
0.0

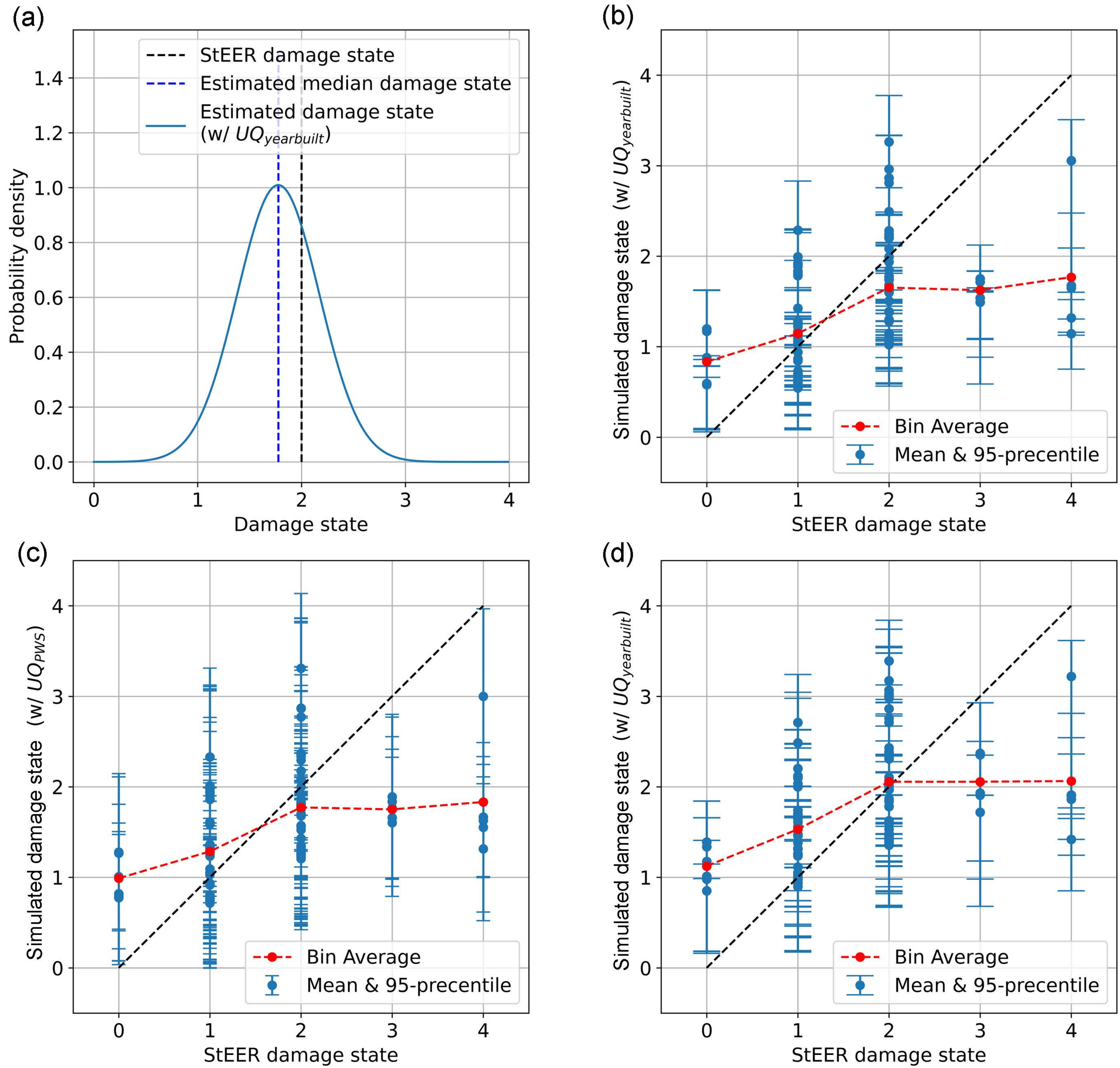
(a)
StEER damage state
Estimated median damage state
Estimated damage state
(w/ $UQ_{yearbuilt}$)
Probability density
Damage state
(b)
Simulated damage state (w/ $UQ_{yearbuilt}$)
Bin Average
Mean & 95-precentile
StEER damage state
(c)
Simulated damage state (w/ UQ_{PWS})
Bin Average
Mean & 95-precentile
StEER damage state
(d)
Simulated damage state (w/ $UQ_{yearbuilt}$)
Bin Average
Mean & 95-precentile
StEER damage state